Müller glia fused with adult stem cells undergo neural differentiation in human retinal models

Sergi Àngel Bonilla-Pons,[a,b] Shoma Nakagawa,[a,1] Elena Garreta Bahima,[c,1] Álvaro Fernández-Blanco,[a,d,1] Martina Pesaresi,[a,d] Justin Christopher D'Antin,[e,f] Ruben Sebastian-Perez,[a,d] Daniela Greco,[a] Eduardo Domínguez-Sala,[a] Raúl Gómez-Riera,[a] Rafael Ignacio Barraquer Compte,[e,f] Mara Dierssen,[a,d,h] Nuria Montserrat Pulido,[c,g] and Maria Pia Cosma [a,d,g,i,j,*]

[a]Centre for Genomic Regulation (CRG), The Barcelona Institute of Science and Technology, C/Dr. Aiguader 88, Barcelona 08003, Spain
[b]Universitat de Barcelona (UB), Barcelona, Spain
[c]Pluripotency for Organ Regeneration, Institute for Bioengineering of Catalonia (IBEC), The Barcelona Institute of Science and Technology (BIST), Barcelona, Spain
[d]Universitat Pompeu Fabra (UPF), Barcelona, Spain
[e]Centro de Oftalmología Barraquer, Barcelona, Spain
[f]Institut Universitari Barraquer, Universitat Autónoma de Barcelona, Barcelona, Spain
[g]ICREA, Pg. Lluis Companys 23, Barcelona 08010, Spain
[h]Biomedical Research Networking Centre On Rare Diseases (CIBERER), Institute of Health Carlos III, Madrid, Spain
[i]Bioland Laboratory, Guangzhou Regenerative Medicine and Health Guangdong Laboratory, Guangzhou 510005, China
[j]CAS Key Laboratory of Regenerative Biology, Guangdong Provincial Key Laboratory of Stem Cell an Regenerative Medicine, Guangzhou Institutes of Biomedicine and Health, Chinese Academy of Science, Guangzhou 510530, China

Summary

Background Visual impairments are a critical medical hurdle to be addressed in modern society. Müller glia (MG) have regenerative potential in the retina in lower vertebrates, but not in mammals. However, in mice, *in vivo* cell fusion between MG and adult stem cells forms hybrids that can partially regenerate ablated neurons.

Methods We used organotypic cultures of human retina and preparations of dissociated cells to test the hypothesis that cell fusion between human MG and adult stem cells can induce neuronal regeneration in human systems. Moreover, we established a microinjection system for transplanting human retinal organoids to demonstrate hybrid differentiation.

Findings We first found that cell fusion occurs between MG and adult stem cells, in organotypic cultures of human retina as well as in cell cultures. Next, we showed that the resulting hybrids can differentiate and acquire a proto-neural electrophysiology profile when the Wnt/beta-catenin pathway is activated in the adult stem cells prior fusion. Finally, we demonstrated the engraftment and differentiation of these hybrids into human retinal organoids.

Interpretation We show fusion between human MG and adult stem cells, and demonstrate that the resulting hybrid cells can differentiate towards neural fate in human model systems. Our results suggest that cell fusion-mediated therapy is a potential regenerative approach for treating human retinal dystrophies.

Funding This work was supported by La Caixa Health (HR17-00231), Velux Stiftung (976a) and the Ministerio de Ciencia e Innovación, (BFU2017-86760-P) (AEI/FEDER, UE), AGAUR (2017 SGR 689, 2017 SGR 926).

Keywords: Retina regeneration; cell fusion; organoids; stem cells; neural differentiation; Muller glia

eBioMedicine 2022;77: 103914
Published online 9 March 2022
https://doi.org/10.1016/j.ebiom.2022.103914

Introduction

Correcting visual impairment resulting from retinal injury or disease is an unmet medical need. The retina is part of the central nervous system and in mammals has very poor regenerative capacity. In contrast, the retina can regenerate efficiently in some cold blood

*Corresponding author at: Centre for Genomic Regulation (CRG), The Barcelona Institute of Science and Technology, C/Dr. Aiguader 88, Barcelona 08003, Spain.
E-mail address: pia.cosma@crg.es (M.P. Cosma).

[1] These authors contributed equally to this work.

Research in context

Evidence before this study

The retina is part of the central nervous system and can be regenerated in some cold blood vertebrates where Müller glia have the capacity to enter the cell cycle in response to damage. Therefore, strategies aiming to awake this regenerative potential in humans represent an attractive medical opportunity. Stem cell therapies can be used to repair degenerating retina either via their paracrine activity or via a regenerative effect, with the final aim of rescuing or replacing the resident damaged neurons. Previous studies in mice showed that adult stem cells can fuse with resident Müller glia and the resulting hybrids exhibited regenerative potential since they could differentiate in photoreceptors or ganglion cells.

Added value of this study

We demonstrated that human Müller glia can fuse with different types of human adult stem cells (mesenchymal stem cells and hematopoietic stem and progenitor cells) giving rise to hybrid cells. We showed that the cell fusion efficiency is enhanced by inflammatory signals and that the activation of the Wnt/beta-catenin pathway increases differentiation of the hybrids into neuronal-like cells, which in turn show electrophysiological properties. Moreover, we observed that the hybrids can engraft and differentiate in growing human retinal organoids.

Implications of all the available evidence

These findings show that the hybrids between Müller glia and adult stem cells might be a promising stem cell-mediated therapy for human retina regeneration and could be used to treat visual impairment. Moreover, these findings show that human Müller glia retain regenerative activity.

vertebrates, such as salamanders and fish.[1] In these vertebrates, MG have the capacity to regenerate the retina by expressing genes common to mitotic, late-stage retinal progenitors[2] and entering the cell cycle in response to damage.[3] Originally believed to serve only as support cells, it is now well established that MG in mammals retain intrinsic stem cell features.[4]

Stem cell transplantation has emerged as a potential therapy for treating retinal degenerations, providing beneficial functions in two, non-mutually exclusive ways: i) cell regeneration and replacement, and ii) a paracrine neuroprotective effect. Among the different types of adult stem cells, mesenchymal stem cells (MSCs) have demonstrated capacity for both tissue regeneration and neuroprotection.[5,6] Further, compelling work has shown that MSCs can adopt both neural and retinal fates.[7-9] Hematopoietic stem and progenitor cells (HSPCs) are another type of stem cell used for cell-based therapies and regenerative approaches; they display an impressive plasticity and can be mobilized *in vivo* from the bone marrow to trans-differentiate or undergo cell fusion with target cells, thereby generating cells of different lineages.[10-13] For instance, mouse HSPCs can migrate into the liver, kidney, heart or retina, and, once on-site, contribute to the regeneration of those tissues.[14-18]

Regeneration mediated by the transplantation of stem cells can be enhanced by the activation of the Wnt/beta-catenin signaling pathway, which *in vivo* results in cellular reprogramming.[19] Over the past few years, we have shown the potential therapeutic use of cell fusion-derived hybrids in models of retinal disease, indicating that cell fusion contributes to the regeneration of retinal neurons.[18,20-23] Further, we showed that after HSPCs are intravitreally transplanted into a variety of retinal-injury models, they fuse with mouse MG (mMG) to generate reprogrammed hybrids.[21,22] Importantly, fusion of the transplanted cells occurs only in the context of tissue damage. Moreover, the hybrids survive and proliferate only when the transplanted HSPCs had been pre-treated with an activator of the Wnt/beta-catenin pathway. Indeed, this signalling pathway enhances the reprogramming of the HSPCs/mMG-derived hybrids, which proliferate and differentiate into functional ganglion cells, amacrine cells or photoreceptors.[21,22]

Finally an important aspect of cell therapy is the observation that stem cells transplanted into the vitreous chamber of the eye migrate toward the site of retinal damage.[21] We recently identified secreted retinal chemokines and, subsequently, defined chemokine-receptor interactions, which can be exploited to optimize stem cell-mediated therapeutic strategies.[24]

On the basis of these data, we hypothesized that fusion-mediated regeneration using adult stem cells could be a treatment for human retinal dystrophies. In the work reported here, we have identified and studied cell fusion events between human MSCs (hMSC) or human HSPCs and human MG in cell culture as well as in retinal organotypic cultures. We found that cell fusion efficiency was increased by inflammatory signals and hybrids undergoing Wnt-dependent activation lose features of MG and transform into neuronal-like cells that display electrophysiological features characteristic of neurons. Finally, when hybrids are injected into human retinal organoids, which constitute an *ex vivo* model of retinogenesis,[25] they engraft and differentiate toward a ganglion cell fate. Overall, these results demonstrate the possibility of using cell fusion-mediated reprogramming of MG in the human retina as a potential therapeutic approach to treating visual impairments.

Methods

Cell lines and tissue culture

ARPE19 cells were purchased from ATCC (RRID: CVCL 0145, ATCC.CRL-2302™, Virginia, USA) and maintained in DMEM/F-12-GlutaMax (Gibco™, Massachusetts, USA) supplemented with 10% fetal bovine serum (FBS) (Thermo Fisher Scientific, Massachusetts, USA), penicillin (100 U/ml) and streptomycin (100 μg/ml) (Thermo Fisher Scientific). CD34+hHSPC were isolated from blood donations from human cord not older than 26 h. CD34+hHSPC cells were isolated by aspirating the dense interphase of the LymphoPrep (Stem Cell Technologies, Vancouver, Canada) solution and with a posterior CD34+ MicroBead Kit UltraPure human column selection (MACS Miltenyi Biotec, NRW, Germany), following manufacturer's instructions. Cells were counted and cryopreserved at one million cells per milliliter in StemSpanTM SFEM (Stem Cell Technologies, Vancouver) supplemented with hIL3 0.02 μg/μl at 1 μl/ml (PeproTech, London, UK), hIL6 0.02 μg/μl at 1 μl/ml (PeproTech), hSCF 0.1 μg/μl at 1 μl/ml (PeproTech), hTPO 0.1 μg/μl at 1 μl/ml (PeproTech), hFlt3 ligand 0.1 μg/μl at 1 μl/ml (PeproTech) in 10% DMSO. For CD34+hHSPC cell infection prior to cell fusion, cells were cultured in suspension at a concentration of one million cells per milliliter in StemSpanTM SFEM (Stem Cell Technologies) supplemented with hIL3 0.02 μg/μl at 3 μl/ml (PeproTech), hSCF 0.1 μg/μl at 3 μl/ml (PeproTech), hTPO 0.1 μg/μl at 3 μl/ml (PeproTech), hFlt3 ligand 0.1 μg/μl at 3 μl/ml (PeproTech). Adipose-derived hMSCs (AD-hMSCs) were a kind gift from Dr. M.J. Hoogduijn (Rotterdam Transplant Group, Department of Internal Medicine, Netherlands). AD-hMSCs were isolated from subcutaneous adipose tissue from kidney donation. Tissues were collected after explicit written informed consent and approval of the Medical Ethical Committee of the Erasmus University Medical Center Rotterdam (protocol no. MEC-2006-190). AD-hMSCs were maintained *in culture* in alpha-MEM without ribonucleases (Gibco™) supplemented with 15% FBS (Thermo Fisher Scientific), 100 μl of 50 ng/ml of human fibroblast growth factor hFGF2 (PeproTech), penicillin (100 U/ml) and streptomycin (100 μg/ml) (Thermo Fisher Scientific). HEK 293 cells for lentiviral production were maintained with DMEM supplemented with 10% FBS (Thermo Fisher Scientific), penicillin (100 U/ml) and streptomycin (100 μg/ml) (Thermo Fisher Scientific). MGs were maintained in 75 cm^2 cell culture flask in DMEM/F-12-GlutaMax (Gibco™) supplemented with 10% FBS (Thermo Fisher Scientific), penicillin (100 U/ml) and streptomycin (100 μg/ml) (Thermo Fisher Scientific) and the medium was changed every two days.

Human retina organotypic cultures

Eyes were donated through a collaboration with "Banc d'Ulls per a Tractaments de Ceguesa" (BUTC). Eyes were from two different origins: from donors classified as non-suitable for cornea transplantation or from eye cups whose cornea was dissected for transplantation and the eye cup was stored at 4°C for less than 48 h to delay retinal autolysis. Explicit, written informed consent for the removal and use of the eyes for diagnostic and research purposes was obtained from patients and/or relatives. The samples received were from donors between 40 and 98 years old. Before retina extraction, the eye was decontaminated by submerging it in BSS (sterile irrigation solution, Alcon, Geneva, Switzerland) for 2 min. Afterwards the globe was submerged in 5% povidone-iodine for 2 min, followed by submersion in sterile sodium thiosulphate 0.1% for 1 min. Lastly, the globe was cleaned by submersion in PBS for 1 min. Retina dissection was performed according to the set-up procedure optimized in our laboratory in collaboration with "Centre d'Oftalmologia Barraquer". Specifically, the globe was placed in a custom-built holder that generates vacuum, providing sufficient internal pressure for an appropriate dissection. The anterior segment of the globe (cornea, iris and crystalline) was removed by making an incision 6 mm away from the iris. This opens a window on the globe, exposing its internal part and making accessible the retina attached to the retinal pigmented-epithelium.[26] Vitreal excess was removed by sponge absorption and the retina was separated mechanically from the RPE with the help of two forceps. The eye globe was then removed from the holder and placed upside-down in a sterile petri dish. In this position, the retina junction with the optic nerve was exposed and could be cut, releasing the retina from the optic cup. Vitreal leftovers and the retina periphery were removed. The central part of the retina was divided in four pieces and every piece was cultured directly into 6 multi-well plates, with the ganglion cell layer facing up, using neurobasal-A medium supplemented with 2% B-27 supplement (50X) (Thermo Fisher Scientific), 1% N2 supplement (Thermo Fisher Scientific), 1% GlutaMax (Thermo Fisher Scientific), penicillin (100 U/ml) and streptomycin (100 μg/ml) (Thermo Fisher Scientific).

Human retina organoid differentiation from hPSC

Human Embryonic Stem Cells (hESCs) (Ese014-A, Spanish Stem Cell Bank ISCIII, SAMEA7778668 BioSamples) were routinely grown in mTeSR1 medium (Stem Cell Technologies) on Matrigel coated plates (Corning, New York, USA) following manufacturer recommendations. hPSC-derived retinal organoids were generated based on a previously described methodology with some modifications [1,2]. Briefly, hPSCs were seeded on Matrigel (Corning) coated plates at 50.000 cells/cm^2

in mTeSR1 medium (day -4). On day 0, when hPSCs cultures reached 80-90% confluency, the medium was changed to pro-neural medium consisting of DMEM/F-12-GlutaMax (Gibco™) supplemented with 1% of N-2 supplement (100X) (Thermo Fisher Scientific), 2% B-27 minus vitamin A supplement (50X) (Thermo Fisher Scientific), 1% MEM NEAA (100X) (Gibco™), penicillin (100 U/ml) and streptomycin (100 μg/ml) (Thermo Fisher Scientific). From day 0 to day 1, the medium was also supplemented with 2% Matrigel. Under these conditions, hPSCs were left to differentiate in 2D monolayer cultures for 16 days, with daily media changes. On day 16, the culture medium was changed to retinal differentiation medium composed of DMEM/F-12 (3:1) supplemented with 2% B-27 minus vitamin A supplement (50X) (Thermo Fisher Scientific), 1% MEM NEAA (100X) (Gibco™), β-mercaptoethanol (50 µM) (Thermo Fisher Scientific), Glutamax (Thermo Fisher Scientific), penicillin (100 U/ml) and streptomycin (100 μg/ml) (Thermo Fisher Scientific). The culture medium was also supplemented with 10 ng/mL of FGF2 (Miltenyi Biotec, RNW, Germany) from day 16 to day 22 of differentiation. From day 16, media changes were performed every other day. On day 25, optic vesicle-like structures were visually identified and mechanically isolated and cultured as floating structures. From day 25, the retinal differentiation medium was additionally supplemented with 5% FBS (Thermo Fisher Scientific), 100 μM taurine (Merck Life Science, New Jersey, USA), and 1:1000 chemically defined lipid supplement (Thermo Fisher Scientific). From this stage onward, the neuroretina start to differentiate generating different neuronal types. From day 25, the medium was changed 3 times a week. Retinal organoids from day 30 onwards were used for micro-injection experiments.

Human retina damage, collection of conditioned medium and cell co-culture experiments

Retinas were cultured up to seven days in Neurobasal-A medium (Gibco™) supplemented with 2% B-27 supplement (50 ×) (Thermo Fisher Scientific), 1% N2 supplement (Thermo Fisher Scientific) and 1% Glutamax (Thermo Fisher Scientific). Retinas were cultured in 2.5 ml, and the medium was replaced every two days. Conditioned medium enriched in secreted factors from the retina was collected at day 1 (as "natural" control condition) and at day 7 of culturing (as "natural" damage condition). Cell co-culture fusion experiments were done by culturing adult stem cells, either AD-hMSC H2B::mRFP or CD34+hHSPC H2B::mRFP. CD34 +hHSPC cells were infected with pHIV-H2B::mRFP for two consecutive days before the co-culture. Human retinas were extracted from the eye globes and, after dissection, were placed in culture for one day. At day one, the medium was replaced and retina were infected with AAV2/ShH10Y445-pRLBP_eGFP. The medium was changed every two days until day 5. In the new medium, the retinas were placed with the ganglion cell layer facing up, and 500,000 adult stem cells expressing H2B::mRFP and resuspended in 50 μl were cultured on top of the retina. After one overnight co-culture, retinas were harvested for further experiments, including FACS and immunohistochemistry.

Western blotting

Cells were cultured until 85% confluency, harvested and washed once with PBS. The wash was done after pelleting cells at 300 rcf for 5 min at room temperature. Cell lysis was performed on ice for 15 min, in RIPA buffer (SIGMA, Missouri, USA) containing protease (SIGMA) and phosphatase inhibitors (SIGMA). The insoluble material was pelleted at 16,000 rcf for 30 min at 4°C. Protein concentrations were determined by Bradford assay (BIO-RAD, California, USA). The protein extract was mixed with 4 × sample buffer (40% glycerol, 240 mM Tris/HCL, pH 6.8, 8% SDS, 0.04% bromophenol blue, 5% beta-mercaptoethanol), denatured at 99°C for 10 min, and briefly centrifuged. The samples were separated by SDS-PAGE on a 10% gel and then transferred to a polyvinylidene difluoride membrane (BIO-RAD). The membranes were blocked with 5% non-fat dry milk (SIGMA) in TBS-Tween 20 (0.1%) (SIGMA) for 60 min and then incubated overnight with primary antibodies in TBS-T with 5% nonfat dry milk, at 4°C. The membranes were then washed three times with TBS-T for 10 min each, incubated with HRP-conjugated secondary antibody (1:2000, Amersham Biosciences NA931V, Amersham, UK) in TBS-T with 5% non-fat dry milk for 60 min, and finally washed three times (10 min each) with TBS-T. The immunoreactive proteins were detected using Pierce ECL Western Blotting Substrate (Thermo Fisher Scientific), and final images were taken with Amersham Imager 600.

RNA extraction and quantitative real-time PCR (qRT-PCR)

The cells were cultured until 85% confluency, harvested, and washed once with PBS. The wash was done by pelleting down the cells at 300 rcf for 5 min at room temperature. The RNA was isolated using RNeasy Mini kit (QIAGEN, Hilden, Germany), according to the manufacturer's protocol. The RNA was then reverse transcribed to cDNA with SuperScript III CellsDirect cDNA Synthesis Kit (Thermo Fisher Scientific). qRT-PCR reactions were performed using Platinum SYBR green qPCix-UDG (Thermo Fisher Scientific) in a LyghtCycler 480 machine (Roche, Basel, Switzerland), according to the manufacturer's recommendations. The oligonucleotides used are listed in Table S1. The data obtained by qRT-PCR were normalized to GAPDH expression. Each

sample was performed in technical triplicates. A minimum of three independent experiments were averaged.

Lentiviral constructs and MSC/CD34+hHSPC/MG infection

The lentiviral construct pHIV-H2B::mRFP was purchased from Addgene (#18982). For the pRLBP_eGFP plasmid, the pRLBP human gene promoter was obtained by reverse transcribing human ARPE19 RNA using SuperScript III CellsDirect cDNA Synthesis Kit (Thermo Fisher Scientific) and then amplified by PCR (using the Phusion hot start high fidelity polymerase, Thermo Fisher Scientific). An eGFP reporter was also extracted by PCR from the pH2B-eGFP plasmid (Addgene #11680) using the Phusion hot start high fidelity polymerase (Thermo Fisher Scientific). SgrAI/AgeI were added to the pRLBP sequence and SgraI/SalI were added to the eGFP obtained by PCR. Both sequences were subcloned into a lentiviral vector with a p1494 backbone giving the final plasmid. For the TUJ1_CRIMSON_Hygro, a similar procedure was followed. Due to the rich GC-content of the TUJ1 promoter region, the TUJ1 promoter was synthetized by the GeneArt company (Thermo Fisher Scientific). The pEF.myc.ER-E2-CRIMSON plasmid was purchased from Addgene (#38770). An SV40_Hygro with its expression driven by a constitutive SV40 promoter, was PCR extracted from a previously generated plasmid (EF1α_HA-Cxcr6-SV40_Hygro). The same restriction enzyme strategy was followed, adding by PCR AgeI/SgrAI, SgrAI/NheI and NheI/SalI to the enumerated fragments. The three fragments were then sub-cloned into a lentiviral vector with a p1494 backbone. pCMV-DR8.2 dvpr (Addgene #8455) and pCMV-VSV-G (Addgene #8454) were used as lentiviral packaging constructs. The oligonucleotides used for the above mentioned fragments are listed in Table S2. Lentiviral production was performed following the RNA interference consortium's (TRC) instructions for lentiviral particle production (http://www.broadinstitute.org/rnai/public/). HEK 293 cells were plated at a known density of 5 × 104 cells per cm2 in p150 plates at day 0. At day 1, the cells were co-transfected with: (A) 19.5 μg pCMV-DR8.2; (B) 10.5 μg pCMV-VSV-G; and (C) 30 μg of the corresponding plasmid construct (H2B::mRFP, pRLBP1_eGFP or TUJ1_-CRIMSON_SV40_Hygro) using a calcium phosphate transfection kit (Clontech, California, USA). At day 2, the medium was replaced with fresh DMEM supplemented with 30% FBS (Thermo Fisher Scientific) and 1% penicillin (100 U/ml) and streptomycin (100 μg/ml) (Thermo Fisher Scientific). The medium was harvested at day 3 and 4 for the viral collection. The viral particles were filtered, ultracentrifuged and aliquoted in batches of 20 microliters for subsequent infection. MGs infected with pRLBP_eGFP and either AD-hMSC or CD34+hHSPC infected with H2B::mRFP were FACS-sorted on the basis of their fluorescent intensity. The pRLBP_eGFP-positive MG cells were then re-infected with TUJ1_CRIMSON_SV40_Hygro and selected by hygromycin resistance (50 μg/ml) starting two days after infection.

Adeno-associated constructs and human retina infection

The labelling of human retina was done through adeno-associated viral infection. Adeno-associated viruses were manufactured by Unitat de Vectors Virals. First, tropism and Müller glia specificity infection experiments were performed using AAV2/8-CMV-GFP. More specifically, Müller glia infective viruses were prepared by modifying the capsid and introducing the generated pRLBP_eGFP construct. The ShH10Y445 capsid plasmid was a kind donation from J. Wijnhold.[27] Unitat de Vectors Virals[28] generated the final adeno-associated virus AAV2/ ShH10Y445-pRLBP_eGFP. Human retinas were infected with 5×10^{10} viral particles. The virus and the medium were replaced daily for 4 days before running the co-culture fusion experiments.

Immunofluorescence and antibodies

Human retinas were washed in PBS for 5 min and fixed by immersion in 4% Paraformaldehyde (PFA) overnight at 4°C. For organoid and retinal sections, serial transversal sections of 5-μm thickness were prepared and processed for immunofluorescence. Briefly, sections were left at 60°C overnight to melt the paraffin, after which they were totally deparaffinized by sequential de-hydration treatment, first with Xylene and then with decreasing ethanol concentrations to re-hydrate the samples. Slices were then placed in a plastic coplin jar with a permeabilization buffer (0.3% Triton X-100 and 0.1 M NaCitrate in PBS) for 1 h at room temperature. Subsequently, the antigen was retrieved by boiling the slices for 4 min in a microwave. After three washes with PBS (for 10 min each), the sections were blocked for 1 h in blocking buffer (3% BSA, 300 μM glycine, 0.03% Triton X-100, 0.01 M NaCitrate in PBS) and then incubated twice overnight at 4°C with the primary antibodies diluted 1:2 in blocking buffer. The sections were washed again the following day and then incubated with secondary antibodies and DAPI (5 mg/ml) for 2 h at room temperature. Three more washes of 15 min each were done before mounting the samples with VectaShield with DAPI (Vector Laboratories, California, USA).

For retinal-piece flat mount, fixed retinas were permeabilized (0.3% Triton X-100 in PBS, 1.5 h at room temperature) and blocked for 1 h at room temperature (3% BSA, 300 μM glycine, 0.03% Triton X-100, in PBS), followed by two overnight incubations with the primary antibodies at 4°C. Retinas were then washed

3 times with PBS for 15 min each and incubated overnight at 4°C with the secondary antibodies and DAPI (5 mg/ml). Subsequently, the sections were mounted with VectaShield with DAPI (Vector Laboratories).

Following flat mount imaging, retina pieces were embedded in paraffin for section re-staining as described above.

Cells plated in 8 multi-well chambers (Lab-Tek Chambered #1.0 Borosilicate Coverglass System) or on a cover glass of 22 mm (VWR, Borosilicate glass 631 – 1089) were immunostained as follows. The cells were washed in PBS for 5 min and fixed by immersion in 4% PFA for 15 min. Directly afterwards, the cells were permeabilized with permeabilization buffer (0.3% Triton X-100 and 0.1 M NaCitrate, in PBS) for 15 min, washed three times for 5 min each, and blocked with blocking buffer for 45 min (3% BSA, 300 μM glycine, 0.03% Triton X-100, 0.01 M NaCitrate, in PBS). The samples were then incubated for 3 h with the primary antibodies diluted 1:2 in blocking buffer. After three washes, of 15 min each, the samples were incubated with the secondary antibodies and DAPI (5 mg/ml) for 1 h one at room temperature. Next, they were washed three more times for 15 min each and then mounted with VectaShield with DAPI (Vector Laboratories).

The following antibodies were used: chicken anti-GFP (1:500; ab13970, Abcam, Cambridge, UK); mouse anti-βIII-tubulin (1:200; ab7751, Abcam); rabbit anti-RFP (1:250; ab62341, Abcam); mouse anti-cralbp (1:200; ab15051, Abcam); rabbit anti-GS (1:200; G2781, SIGMA); mouse anti-TUJ1 (1:200; MAB1637, Millipore, Massachusetts, USA); rabbit anti-Pax6 (1:200; ab5790, Abcam); mouse anti-GFAP (1:200; MAB360, Millipore); mouse anti-Sox9 (1:200; MA5-17177; Thermo Fisher Scientific); mouse anti-rhodopsin (1:200; MAB5356, Millipore); mouse anti-calretinin (1:200; MAB1568, Abcam); rabbit anti-dsRed (1:200, 632496, Takara, Kyoto, Japan) and rabbit anti-IBA1 (1:200; 019-19741, Fujifilm, Ohio, USA). All secondary antibodies were from Molecular Probes (Thermo Fisher Scientific) and diluted 1:1000 in PBS. The secondary antibodies used were: alexa-fluor® 488 goat anti-chicken (1:1000, A32731), alexa-fluor™ 488 goat anti-mouse (1:1000, A32723), alexa-fluor™ 568 goat anti-rabbit (1:1000, A-11011), and alexa fluor™ 647 goat anti-mouse (1:1000, A32728). DAPI (5 mg/ml) was used to stain for cell nuclei. For all samples, images were taken using either Leica laser SP5 or SP8 confocal microscopy systems.

Immuno-TUNEL assay and frozen tissue sections

Human retina divided in pieces were washed in PBS for 5 min and fixed by immersion in 4% PFA overnight, at 4°C. Three washes with PBS of 20 min each were done immediately after, to later proceed to the cryoprotection by immersing the samples in rising concentrations of sucrose: 15% sucrose for 30 min, 20% sucrose for 1 h, and 30% sucrose overnight at 4°C. Samples were then embedded in OCT and cryo-sectioned in sections of 10-12 μm. For the immuno-TUNEL staining, immunostaining was performed with primary antibodies as described previously, then after the primary incubation, the TUNEL staining was carried out. TUNEL staining was performed following manufacturer's instructions (In Situ Cell Death Detection Kit, TMR Red, Merck). Briefly, human retinas chopped in pieces, already permeabilized and blocked from the immunostaining, were incubated with the TUNEL reaction mixture at 37° C in a humidified chamber, for 1.5 h. Directly afterwards, they were incubated with the secondary antibodies and DAPI (5 mg/ml) for the final immunostaining step. Lastly, samples were mounted with VectaShield with DAPI (Vector Laboratories). Images were taken using the Leica laser SP8 confocal microscopy system.

Flow cytometry analysis

For hybrid identification, flow cytometry of human retinas chopped in pieces and co-cultured with adult stem cells was based on the protocol described in section 2.4. Retinas chopped in pieces were disaggregated mechanically and chemically with 0.05% Trypsin-EDTA (1X) (Gibco™) for 20 minutes, filtered through a 70-μm filter, pelleted, and resuspended in 1 ml PBS supplemented with 2% FBS (Thermo Fisher Scientific) and DAPI (5 mg/ml) before analysis. Cell fusion events were detected by first excluding the dead DAPI+ cells and the double GFP and RFP cells, as detailed before. Flow cytometry analysis was performed using LSR Fortessa (Becton Dickinson, New Jersey, USA) with FACS-Diva software (Becton Disckinson) and FlowJo software.

FACS sorting analysis

Cell fusion was performed as described in the section 2.14 . In this case, a more refined selection was done, to obtain a cleaner population of sorted hybrids, for subsequent experiments. The entire population of fused cells was incubated with HOESCHT 33342 (Thermo Fisher Scientific) at 37°C for 45 min to determine the DNA content of the cells. The cells were then pelleted down and resuspended in PBS with To-ProTM-3 Iodide (Thermo Fisher Scientific) to determine cell viability. Before sorting, the cells were filtered with a 70-μm filter. Double GFP+RFP+ cells, 4n cells, and higher ploidy cells were sorted for subsequent experiments. Cell sorting was performed using a BD Influx sorting machine (Becton Dickinson) and analyzed with the FlowJo software.

Time-lapse imaging

FACS-sorted hybrids were plated on Time-Lapse poly-ornitine/laminin coated Thermo Scientific Nunc Lab-Tek chambered coverglass. After 3 h, when the cells

were attached to the plate, they were treated with the differentiation medium: 20 ng/ml human fibroblast growth factor hFGF2 (PeproTech) and 50 μM Notch inhibitor DAPT (SIGMA)[29] or control conditions (DMSO and PBS). Images of the process were acquired on Andor Revolution XD inverted Olympus microscope. The images of the cells were taken up to 24 h, in an incubator chamber at 37°C and 5% CO2.

Co-culture and cell fusion

Co-culture and cell fusion experiments were adapted from previous work in our laboratory.[30] To mimic damage conditions, human ARPE19 cells were grown in monolayer. In parallel, MGs pRLBP_eGFP and hMSC H2B::mRFP were cultured to 75–80% confluency. At day 1 of fusion, the ARPE19 monolayer was exposed to either 1 mM NMDA damage or PBS control. At day 0, cells were separately detached and co-cultured in suspension for 45 min, in a volume of 200 microliters, in a 1:1 ratio, with a maximum of 500,000 cells per cell fusion partner. Cells were then plated in a T75 cell culture flask (Corning) and left in culture overnight. On day 1, hybrids were detached and prepared for FACS cell sorting and for the following experiments.

In vitro patch clamp

Cells to patch (MGs or GFP+RFP+ 4n hybrids) were placed in a recording chamber in a Olympus BX51WI microscope. Electrophysiological recordings were acquired at 20kHz with Multiclamp 700B (Axon Instruments) and were digitized at 16 bits (Axon 1550B Digidata, Molecular Devices). Patch pipettes of borosilicate glass were pulled (Sutter P-97) and filled with internal solution for whole-cell somatic current clamp recordings (135 mM KMeSO4, 10 mM KCl, 10 mM HEPES, 5 mM NaCl, 2.5 mM ATP-Mg, 0.3 mM GTP-Na). The intracellular solution was adjusted to pH 7.2 and displayed osmolarity values in the interval 285–295 mOsm. Pipette resistance ranged between 5–7 MΩ, pipette capacitance ranged from 7 to 7.5 pF and series resistance ranged between 10-40 MΩ. The electrophysiological properties of the patched cells were obtained in current-clamp configuration by applying a sequence of hyperpolarizing and depolarizing current pulses and were analyzed with Clampfit 9.

In vitro live cell calcium imaging

The intracellular calcium (Ca^{2+}) oscillations were studied using Fluo4-AM (Thermo Fisher Scientific). The cells were incubated with Fluo4-AM 2 µM for 5 minutes in DMEM media (Gibco^{TM}), at room temperature. After incubation, the excess Fluo4-AM was removed by replacing the DMEM media. After incubation, the wells were mounted on a Leica SP5 STED microscope. The recordings were made at 37°C and 5% CO_2. Fluo4-AM (Thermo Fisher Scientific) was excited at 488 nm and its fluorescence emission was collected at 525 nm using a 40x oil immersion objective. The images were sampled at a rate of 1 Hz for 2 minutes both for basal activity and after ATP bath application (10 µM). The images were stored as image stacks containing time-lapse images and analyzed using a custom Matlab script. The fluorescence traces were extracted from manually segmented regions of interest corresponding to cell bodies and were presented as relative changes in fluorescence ($\Delta F/F$). Calcium fluctuations were measured by *in house* developed code kindly provided by Dr. Gertrudis Perea and Dr. Julio Esparza.[31]

Human retina organoid micro-injection and imaging

Human retina organoids were detached from the cell culture dish by dissecting with a needle. The organoids were then transferred to a microinjection dish into M2 medium (SIGMA) drops covered with NidOil^{TM} (Nidacon, Gothenburg, Sweden) and were micro-injected with GFP+RFP+ 4n hybrids by holding them with a holding pipette and micro-injecting with a manufactured sharpened injecting pipette of 70 μm. The organoids were micro-injected with 20-25 cells per injection. Once injected, each single organoid was mounted in a bed of low melting agarose base and confined in a capillary for the mesoscopy imaging. Once set, the imaging chamber was loaded with DMEM/F-12-GlutaMax (Gibco^{TM}) without phenol red, supplemented with 1% N-2 supplement (100X) (Thermo Fisher Scientific), 1% B-27 supplement (50X) (Thermo Fisher Scientific), 1% MEM NEAA (100X) (Gibco^{TM}), penicillin (100U/ml) and streptomycin (100 μg/ml) (Thermo Fisher Scientific) and imaged for 12 h at 5% CO2 and 37 °C. Images were taken with MuViSPIM microscope (LuXendo). The organoids were also fixed, sectioned, and immunostained as described before.

Image processing and quantification

All immunofluorescence images were processed with the FiJi ImageJ software. The quantifications were based on the analysis of at least three biological replicates. For each sample analyzed, at least three random fields were analyzed. The quantification of the cells labelled positive (TUNEL+ or marker specific+) was performed manually with the cell counter tool.

The GFP decrease of the sorted 4n hybrids pRLBP_eGFP+/H2B::mRFP was calculated using a code developed in house. The decrease of GFP values was expressed as percentage of decrease, normalized to the initial GFP value for every single cell analyzed, ± SEM.

The projection length of the hybrids was quantified by identifying the cells and defining their cytoplasmic edge to skeletonize them using a pipeline implemented

in the CellProfiler software.[26] The cell nucleus detection was done by setting the threshold of Minimum Cross_-Entropy and the edge by Sobel filter. Subsequently, we applied the Watershed_Gradient method to define the cell. Once the cell was defined, we obtained a single-pixel-wide skeleton using the Morphological_Skeleton module. Then we calculated the shortest path between the two most distal vertexes using the FiJi Image software with the plugin analyze skeleton (2D/3D).[32,33]

Reagents validation

hMG cells were primary isolated and characterized as exposed in the manuscript. AD-hMSC was a kind gift from Dr. M.J. Hoogduijn. This primary cell line was validated in previous publications.[34] ARPE19 cells were purchased from a leading company and were previously validated. Additionally, all the cultured cells were routinely inspected, accounting for their morphology and doubling time. All the antibodies were purchased from leading companies and have a specific labeling or molecular weight according to the data sheet provided by the vendors.

Statistical analysis

As specified in the figure legends, the data are presented as mean ± SEM or scattered points (with line at median). All statistical tests and graphs were generated using the Prism 6.0 software (GraphPad, San Diego, CA). The FACS analysis of the hybrids was defined by odd ratio, indicating that an event happens after a treatment (co-culture or not co-culture) and not by chance. Odd ratios follow the formula below. If OR $\geq$ 1, then the identified events are due to the treatment conditions.

		Outcome	
		Yes	No
Treatment	Yes	A	B
	No	C	D

$$OR = (AxD)/(BxC)$$

Different statistical analyses were run depending on the experimental setup, including the Mann–Whitney test, the two-tailed Student's t-test, the one-way ANOVA Dunnett's post-hoc test and the two-way ANOVA Tukey's post-hoc test. In all cases, a P-value < 0.05 was considered significant (*, P <0.05; **, P <0.01; ***, P <0.001; ****, P <0.0001; ns = not significant).

Ethics

Retinal organotypic experiments and hMG experiments were performed after explicit, written informed consent for the removal and use of the eyes for diagnostic and research purposes was obtained from patients and/or relatives. CD34+hHSPC were isolated from human cord blood donations under "Parc de Salut Mar – Clinical Research Ethics Committee" approval with number 2016/6950/I

Role of funding source

This study was supported by different funding agencies. We acknowledge and thank the support received from all of them in the Funding section. The funders were not involved neither in the study design, data collection, interpretation and analysis of the data nor in the writing of the manuscript.

Results

The structural integrity of human retina is preserved for few days in organotypic cultures

To investigate whether hMSCs can fuse with MG in an intact retina, we first examined how long a human retina can be preserved in an organotypic culture. Briefly, around 48h after death of the donors, retinas were dissected using modifications to a previously published method[35], and each retina was divided into four pieces and cultured for 1, 3, 5, or 7 days, respectively. Hematoxylin and eosin (H&E) staining revealed a progressive loss of structural integrity, which was more severe in the periphery than in central retina and most obvious at days 5 and 7 (Figure S1a). We then quantified cell death in central retinas over the 7 days of culture using the terminal deoxynucleotidyl transferase dUTP nick end-labeling (TUNEL) assay, which identifies apoptotic cells (Figure 1a, red). In the same sections, we also labeled MG by immunostaining for the MG marker, cellular retinaldehyde–binding protein (CRALBP) (Figure 1a, green). Qualitative inspection of TUNEL+ cells showed increasing cell death over the seven days, consistent with the loss of tissue architecture. Quantitatively, and in agreement with the degrading retinal architecture, there was a significant increase in the normalized number of TUNEL+ cells at 5 and 7 days (Figure 1a and b). Finally, to quantify the death of MG, we calculated the percentage of double-positive cells, i.e., CRALBP+ TUNEL+, versus the total number of CRALBP+ MG. This showed a significant, and progressive increase in the number of dying MG at days 5 and 7 (Figure 1a and 1b). Considering these results, in the subsequent cell-fusion experiments we decided to use cultures up to a maximum of five days.

Cell-to-cell fusion between MG and adult stem cells occurs in human retinal organotypic cultures

In mice, transplanted bone marrow–derived stem cells can fuse with mMG *in vivo*.[21] To determine if similar cell-to-cell fusion can occur in human retinas, MG within the explanted retinas and AD-hMSCs were

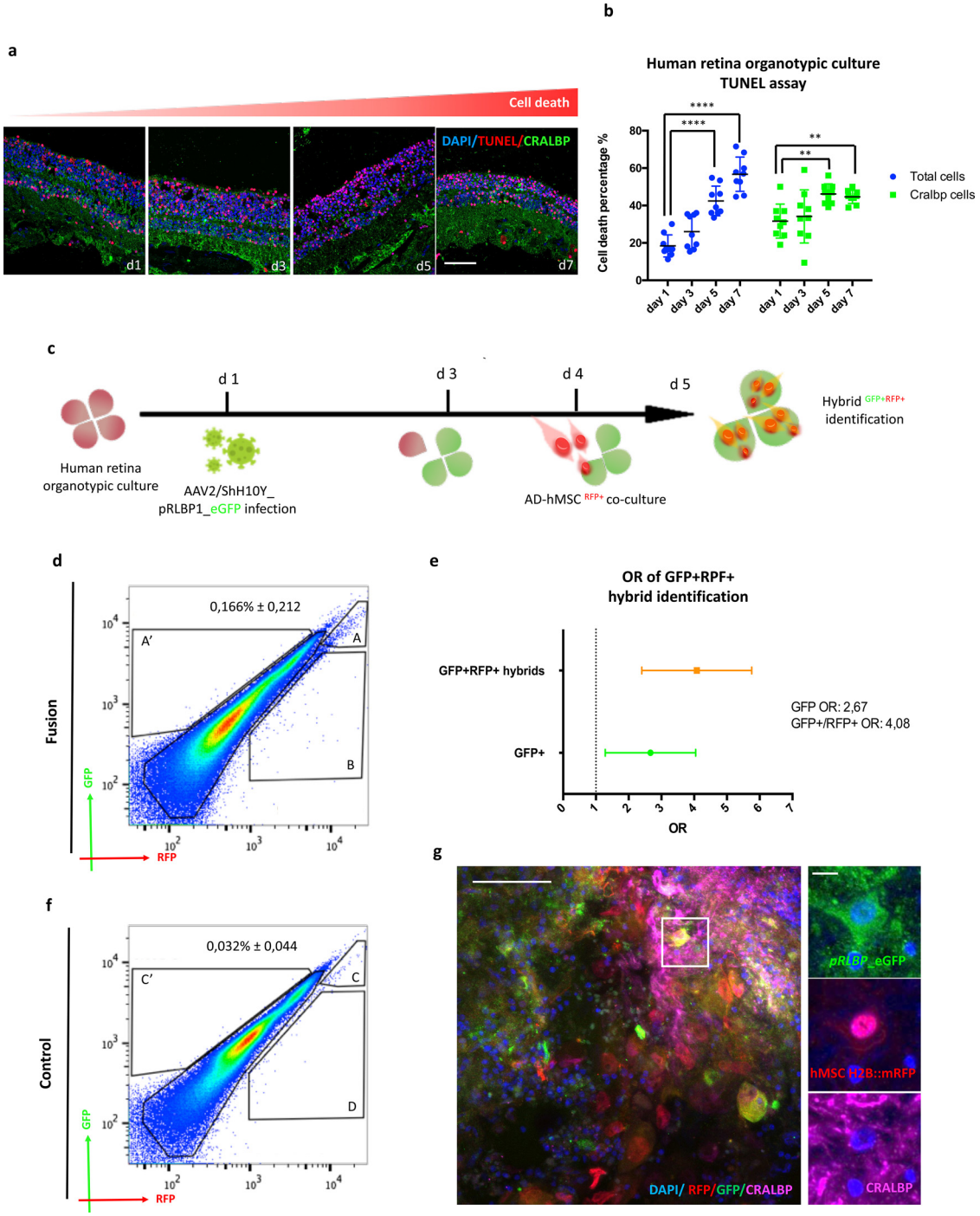

Figure 1. Identification of cell fusion between AD-hMSC and MG in a human degenerating retina organotypic culture. (a) TUNEL assay combined with immunostaining against CRALBP to specifically label MG in human organotypic cultures up to 7 days of culturing. TUNEL+ cells are shown in red; CRALBP+ cells, in green; DAPI-stained cell nuclei, in blue. d1, day 1; d3, day 3; d5, day 5; d7, day 7. (b) Significant increase of cell death was observed from day 5 onwards. The percentage of TUNEL+ (blue) and TUNEL+ CRALBP+ cells (green) is plotted. Data are presented as individual values, mean ± standard error mean (SEM) from n = 3 independent experiments, from 3 independent donors (quantifying 3 random fields per time point and experiment). **P < 0.01; ****P < 0.0001 (Unpaired t-test). (c) Experimental scheme of cell fusion experiments after co-culturing AD-hMSCs expressing H2B::mRFP (AD-hMSC^{RFP}) on top of AAV2/ShH10YpRLBP_eGFP infected retina. The procedure was carried out during the first 5 days of organotypic cultures. (d and f) Representative FACS plots to identify fusion events between human retina cells infected with AAV2/ShH10Y-

initially transfected with fluorescent reporter constructs. Adeno-associated viruses (AAV) can efficiently infect neurons in human retinas.[36,37] To label MG in human retinas, we used the ShH10Y modification in the AAV capsid, as it has been shown to increase specificity for infecting MG cells.[27] We engineered the AAV2 capsid to express the ShH10Y modification and cloned *eGFP* under the control of the MG-specific promoter for retinaldehyde binding protein (*pRLBP*). The ability of AAV2/ShH10Y-pRLBP_eGFP to selectively infect MG was confirmed by immunostaining the infected cells, $MG^{AAV\text{-}GFP}$, in which immunostaining for GFP colocalized with immunostaining for CRALBP (Figure S1b). As expected, the nuclei of AAV-GFP+ cells were in the Inner Nuclear Layer (INL), and GFP+ processes extended across the retinal layers. We then further validated the GFP expression by flow cytometry. Analyzing retinas infected with AAV2/ShH10Y pRLBP1_eGFP by Spectra view FACS showed that infected human retinas, but not control retinas, contained GFP+ cells (Figure S1c). In parallel, AD-hMSC were transduced with a lentivirus vector carrying the histone H2B tagged with the monomeric red fluorescence protein (mRFP) (termed $AD\text{-}hMSC^{H2B::mRFP}$) (Figure S1d).

We then tested the ability of AD-hMSCs to fuse with MG in the organotypic cultures (Figure 1c). First, the retina was divided in four equal parts and cultured. The following day (day 1) three parts of the retina were infected with AAV2/ShH10Y-pRLBP_eGFP and one served as uninfected control. Two days after infection (day 3), retinas were washed and cultured with fresh medium. On day 4, $AD\text{-}hMSC^{H2B::mRFP}$ were co-cultured with the retinas containing infected $MG^{AAV\text{-}GFP}$. After overnight co-culture (day 5), the samples were disaggregated and analyzed by FACS. We found GFP+RFP+ hybrids in the $MG^{AAV\text{-}GFP}$ infected retinas co-cultured with $AD\text{-}hMSC^{H2B::mRFP}$ (Figure 1d). Although a clearly defined population of GFP+RFP+ cells was evident, the control retinas also gave rise to a small population of GFP+RFP+ cells (Figure 1f), likely due to autofluorescence of apoptotic cells present in the retinas. To verify that the GFP+RFP+ hybrid cells were the results of cell fusion, we performed an odds ratio (OR) analysis.[38] In brief, OR is a measure of the association between an experimental condition (co-culture of AAV2/ShH10YpRLBP_eGFP infected retina with $AD\text{-}hMSC^{H2B:mRFP}$) and the outcome phenotype (the presence of GFP+RFP+ hybrids); OR>1 indicates an increased occurrence of the outcome following a given exposure (Figure 1e). The results showed that OR values from both GFP+ and GFP+RFP+ hybrids were higher than 1 (with values of 2.67 and 4.08, respectively), indicating that these populations were obtained through the experimental conditions and confirming the presence of a population of GFP+RFP+ hybrids. In addition, the AAV2/ShH10Y-pRLBP_eGFP−infected retinas (GFP^+) co-cultured with $AD\text{-}hMSC^{H2B:mRFP}$ (RFP+) were immunostained with antibodies against GFP, RFP and CRALBP. At day 5, the presence of hybrids from the fusion of $MG^{AAV\text{-}GFP}$ with $AD\text{-}hMSC^{H2B::mRFP}$ was confirmed by colocalization of all three markers (GFP+RFP+CRALBP+) in whole mount preparations (Figure 1g).

Cell-to-cell fusion in vitro is enhanced by pro-inflammatory signals but is independent of Wnt

Having identified hybrids in the organotypic cultures, we next sought to study their phenotype and differentiation potential in a separate *in vitro* system. We purified MG from human retinas by slightly modifying a previously published protocol.[39] To confirm the efficient purification of MG, we transduced the isolated cells with a lentivirus vector carrying eGFP under the MG-specific promoter *pRLBP* and also expressing two nuclear localization signals (2 × NLS) (Figure S2a). We then sorted the GFP+ cells and analyzed the expression of the glial markers, GLUTAMINE SYNTHASE (GS) and CRALBP, as well as of the neural-progenitor marker, PAX6, by both immunostaining (Figure S2b) and Western blot (WB) analysis (Figure S2c). WB analysis was carried out with samples obtained at three different passages of the MG^{GFP} cells. The human adult retinal pigmented-epithelium cell line, hARPE 19, was used in parallel, as a negative control for the expression of GS and PAX6 and as a positive control for CRALBP. WB analysis showed the expression of GS, CRALBP and PAX6 in MG^{GFP} (Figure S2c). In addition, GFP co-localized with GLIAL FIBRILLARY ACIDIC PROTEIN (GFAP), which labels astrocytes, another type of glial cells. In contrast, GFP did not co-localize with makers for non-glial cells, such as the IONIZED CALCIUM BINDING ADAPTOR MOLECULE 1 (IBA1), which labels microglia, the ganglion cell marker CALRETININ, or the rod photoreceptor marker RHODOPSIN

pRLBP_eGFP and $AD\text{-}hMSC^{H2B::mRFP}$ cells. (d) retina organotypic culture infected with AAV2/ShH10Y-pRLBP_eGFP. A: percentage of GFP+RFP+ cells, A': percentage of GFP+ cells; B: percentage of total cells. (f) control retina organotypic culture; C: percentage of GFP+RFP+ cells; C': percentage of GFP+ cells; D: percentage of total cells. (e) Odds ratio (OR) calculation of GFP+ cells and GFP+RFP+ hybrids identified by FACS analysis using the formula: OR = (A*D)/(B*C) & (A'*D)/(B*C') in infected (d) and control retinas (f). Data are presented as individual values, with mean ± SEM from n = 3 independent experiments from 3 independent donors. (g) Immunostaining of retinal whole mount after organotypic culture using antibodies against GFP (green), RFP (red), and CRALBP (magenta). Hybrids were identified in retinas infected with AAV2/ShH10Y-pRLBP_eGFP and co-cultured with $AD\text{-}hMSCs^{H2B::RFP}$. Scale bar = 100 μm.

(Figure S2d). These results confirmed the efficient isolation of MG cells.

We previously showed an increase in the efficiency of cell fusion–mediated reprogramming in mouse retinas upon activation of the Wnt/beta-catenin pathway in the HSPCs prior to transplantation.[21,22] We therefore activated the Wnt/beta-catenin pathway in AD-hMSCs using Chiron, a specific inhibitor of GSK3,[40] which triggers a downstream cascade of events resulting in the upregulation of several transcription factors, including *AXIN2* and *SOX9*.[41] We evaluated the expression levels of these transcription factors by quantitative real-time PCR (q-PCR) after treating AD-hMSCs with three different concentrations of Chiron (1, 3 and 6 μM). We observed increased RNA expression of *AXIN2* and *SOX9* at 6 μM Chiron treatment, which suggested the activation of the Wnt/beta-catenin pathway at this drug concentration (Figure S2e). Notably, Chiron activation did not result in any change in cellular morphology (Figure S2f). Additionally, we analyzed the AD-hMSCs to ensure that the Chiron treatment did not affect their phenotype. MSCs must present the surface markers CD90, CD73 and CD105, but not CD34 and CD45.[42,43] Indeed, AD-hMSCs expressed CD90, CD73 and CD105 surface markers in both control and Chiron-treated cells. As expected, neither CD34 nor CD45 were expressed (Figure S2g).

In mice, cell fusion is promoted by NMDA-mediated tissue injury and the consequent inflammatory response.[21,22] Therefore, we determined whether NMDA treatment of hARPE-19 cells could induce a pro-inflammatory response.[44,45] After 24 h of NMDA treatment, the expression level of the pro-inflammatory factor *IL1B* and the excitotoxic marker *FOXP3* were both increased (Figure S3a), with no morphological changes in the cells (Figure S3b). In contrast, the senescence-associated gene *SIRT1* was not significantly increased. We also treated hARPE19 cells with H_2O_2, a strong pro-inflammatory treatment, and observed very high cell death along with high upregulation of *SIRT1, IL1B* and *FOXP3* (Figure S3c-d). Previous reports showed that a severe damage could be counterproductive for its effects on reprograming and regeneration.[46] Therefore, for all the subsequent experiments, we used NMDA, which does not cause severe inflammation.

We next studied cell-to-cell fusion between isolated MG^{GFP} and AD-$hMSC^{H2B::mRFP}$. In addition, since we previously demonstrated cell fusion of mMG with bone marrow-derived HSPCs in mice,[21,22] we also tested the fusion with human bone marrow–derived CD34+ hHSPCs. For this purpose, we generated CD34+ $hHSPC^{H2B::mRFP}$ cells upon transduction with a lentivirus vector carrying the histone H2B tagged with mRFP (Figure S3e) and then tested their fusion with MG^{GFP}.

The conditioned medium harvested from NMDA-treated or PBS-treated hARPE19 (herein named NMDA-RPE medium and PBS-RPE medium, respectively) was used to co-culture MG^{GFP} with either AD-$hMSC^{H2B:mRFP}$ or CD34+ $hHSPC^{H2B::mRFP}$. We also used Chiron to activate the Wnt/beta-catenin pathway in AD-$hMSC^{H2B:mRFP}$ (Figure 2a). After co-culture, the GFP+RFP+ 4n hybrids were purified by FACS. Furthermore, we analyzed the DNA content using HOECHST 33342 as an additional selection method, since the hybrids were expected to be 4n (Figure 2b). Indeed, after cell fusion, 4n hybrids can be isolated as previously shown in mice.[20,21,22,47] FACS analyses showed, relative to the PBS-RPE control, that the NMDA-RPE media significantly increased the percentage of GFP+RFP+ 4n hybrids (Figure 2c-2e), indicating that pro-inflammatory signals enhanced the efficiency of cell fusion. Next, we asked whether we could observe comparable changes in the efficiency of cell fusion by substituting the NMDA-RPE and PBS-RPE media with media collected from the organotypic cultures, at day 1 and day 7 (D1, D7), respectively. We infer that at D7, pro-inflammatory signals released by the cultured retina are stronger than at D1.[48,49] Indeed, cell fusion was greater when cells were cultured in the presence of the D7-medium compared to the D1-medium (Figure 2f-2h). Thus, the natural pro-inflammatory state of the retina is also capable of enhancing the efficiency of cell fusion.

We then activated the Wnt/beta-catenin in AD-$hMSC^{H2B:mRFP}$ by treating the cells with Chiron. As indicated above, we observed an increase in cell fusion when the cells were cultured in the presence of NMDA-RPE or in the D7-medium (Figure 2e and 2h). Chiron treatment did not produce significant changes neither for the cells cultured in PBS-RPE or the D1-medium, nor for those grown in NMDA-RPE or the D7-medium (Figure S3f and S3g). Taken together, we concluded that the efficiency of cell fusion was enhanced only by the pro-inflammatory signals and not by the Wnt/beta-catenin pathway activation.

Finally, we found a significant increase in GFP+RFP + 4n hybrids when we evaluated the fusion of CD34 +$hHSPC^{H2B::mRFP}$ with MG^{GFP} cultured in the presence of the NMDA-RPE medium as compared to PBS-RPE (Figure S3h). The percentage of hybrids was comparable when either CD34+$hHSPC^{H2B::mRFP}$ or AD-$hMSC^{H2B:mRFP}$ were co-cultured with MG^{GFP} in the NMDA-RPE medium (Figure S3i).

GFP+RFP+ 4n hybrids can differentiate towards a neuronal-like phenotype

Previous data from our laboratory showed that in the mouse retina, the activation of the Wnt/beta-catenin pathway in transplanted stem cells induces increased reprogramming of the hybrids, which in turn can differentiate into retinal neurons.[21,22] Thus, we tested whether GFP+RFP+ 4n hybrids differentiate toward a neuronal lineage upon Chiron-dependent activation of

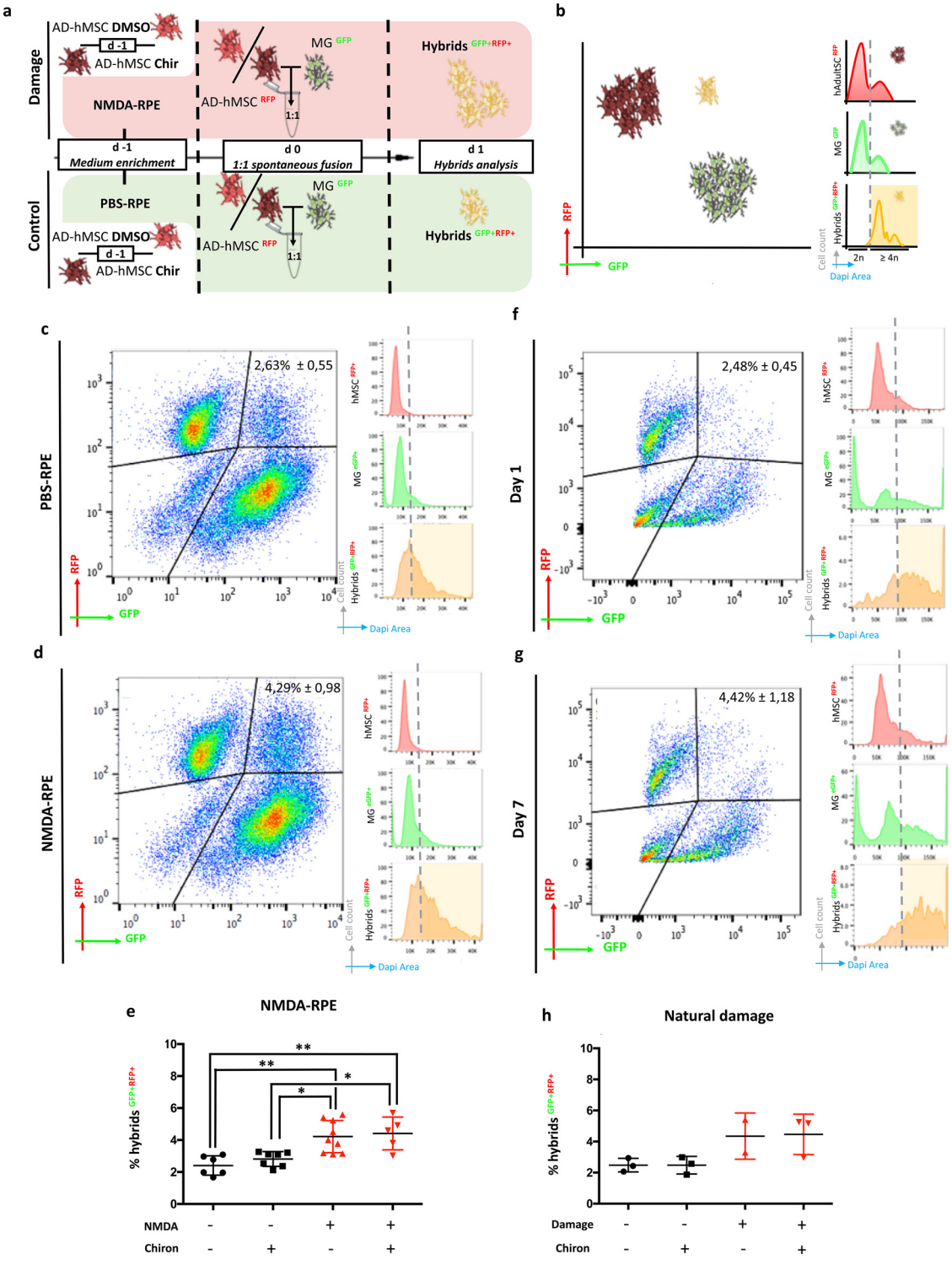

Figure 2. Cell fusion efficiency between hMSCs and MG is enhanced by pro-inflammatory signals, but not by the Chiron-mediated Wnt/beta-catenin pathway activation. (a) Scheme of the fusion protocol for in vitro fusion assessment using NMDA- (as a damage, light red) or PBS- (as a control; light green) conditioned media. The fusion of MG^{GFP} with AD-$hMSCs^{RFP}$ is performed using Chiron-activated AD-hMSCs (AD-hMSC Chir) or control cells (AD-hMSC DMSO). (b) Scheme showing the cell-sorting strategy to identify GFP +RFP+ 4n hybrids by FACS analysis. Light yellow window, GFP+RFP+ 4n are sorted for subsequent analyses. (c and d) Representative FACS plots of sorted hybrids cultured in PBS-RPE medium (c) or in NMDA-RPE medium (d). The GFP+RFP+ population was gated

the Wnt/beta-catenin pathway in the AD-hMSC$^{H2B:mRFP}$ cells. Consistent with this, we also tested whether MG^{GFP}-specific genes were silenced, as evidenced by diminished GFP expression driven by the *pRLBP* promoter. We first cultured GFP+RFP+ 4n hybrids generated after fusion of AD-hMSC$^{H2B:mRFP}$ with MG^{GFP}, using NMDA-RPE media supplemented with 20 ng/ml human fibroblast growth factor 2 (hFGF2) and 50 μM of a NOTCH inhibitor (DAPT), to induce ganglion cell differentiation[29] (Figure 3a). Interestingly, we observed a neural-like phenotype only when they had been cultured in differentiation medium and the AD-hMSC$^{H2B:mRFP}$ cells used in the fusion experiments were treated with Chiron. They displayed an elongated soma and processes, which resemble podocyte-like structures and thin, axon-like projections (Figure 3b, lower row, and Supplementary video 1). In contrast, when cultured in differentiation medium, the hybrids generated with AD-hMSC$^{H2B:mRFP}$ without Chiron-treatment displayed aberrant podocyte-like structures as well as a significant soma expansion, suggesting that in the absence of Wnt/beta-catenin activation, if they were forced to differentiate, they likely did it aberrantly (Figure 3b, upper row, and Supplementary video 2). GFP+RFP+ 4n hybrids exposed to non-differentiation conditions did not show any major morphological change (Figure 3c and Supplementary video 3 and 4). We then quantitatively determined the length of the projections of GFP+RFP+ 4n hybrids. We observed a neural-like phenotype and extended projections only in the hybrids cultured in differentiation medium obtained after fusion of AD-hMSC$^{H2B:mRFP}$ cells treated with Chiron (Figure 3d and supplementary videos 5-8).

Next, we quantified GFP fluorescence intensity over time in the hybrids generated with AD-hMSC$^{H2B:mRFP}$ with or without Chiron-treatment and cultured in differentiation or non-differentiation conditions (Figure 3e and 3f). GFP silencing can be considered a proxy for MG identity-loss following fusion. Fluorescence intensity was normalized to the initial fluorescence of each cell imaged at 1 h after the start of the time course, set as 100% of GFP intensity. All hybrids cultured in the differentiation media showed a significant decrease of GFP intensity, which dropped to 40% at 24 h (Figure 3e). Hybrids cultured in the non-differentiation media showed no significant decrease of GFP intensity, although in those formed with AD-hMSC$^{H2B:mRFP}$ without Chiron and cultured in NMDA-RPE medium, GFP expression was downregulated (Figure 3f).

Under differentiation conditions, a decrease in GFP intensity was evident by 4 h when AD-hMSC were subjected to Chiron-mediated activation of the Wnt/beta-catenin pathway; when instead the Wnt/beta-catenin pathway was not activated, GFP levels were significantly decreased only at 12 h (Figure 3e). The rapid decrease in GFP intensity induced by Chiron treatment of the AD-hMSC suggests that the activation of the Wnt/beta-catenin pathway accelerates the loss of MG identity.

In vitro differentiated hybrids show electrophysiological characteristics of maturing neurons

When cultured in differentiation conditions, the GFP+RFP+ 4n hybrids generated after fusion of AD-hMSC$^{H2B:mRFP}$ with MG^{GFP} using NMDA-RPE media showed a ganglion cell–like phenotype (Figure 3b and d and supplementary videos 1 and 5). To determine if the observed morphological differentiation also resulted in neuronal-like electrophysiological properties, we used whole-cell patch clamp techniques to characterize the electrophysiological response of GFP+RFP+ 4n hybrids cultured for two days under differentiation or non-differentiation treatment (Figure S4a). We measured the resting membrane potential, which is defined as the electrical potential difference across the membrane, and the membrane resistance, which is dependent on the number of open ion channels in the membrane[50]. FACS-sorted MG, differentiated for two days, were used as treatment control, and MG not subjected to FACS sorting, cultured in differentiation medium, were used as the patch clamp technical control. We observed that the FACS procedure itself sensitized the cells, both the hybrids and MG controls (Figures 3g and 3h). We characterized all the differentiated hybrids and their respective non-differentiated controls (Figure S4b). Only the hybrids - obtained from the fusion of AD-hMSC treated with Chiron and cultured in NMDA-RPE medium - displayed a resting membrane potential upon differentiation comparable to differentiated neurons (Figure 3g). Indeed, upon Wnt activation of the AD-hMSCs used for the cell fusion, the obtained hybrids showed a significantly lower resting membrane potential, as low as -45mV, compared with both the

from the total population. Hybrids with 4n or higher ploidy (orange squares) were gated from GFP+RFP+ cells. (e) FACS data quantification of GFP+RFP+ 4n hybrids from PBS-RPE or NMDA-RPE media (either with or without Chiron-dependent Wnt/beta-catenin pathway activation of the AD-hMSC). Data are presented as individual values, mean ± SEM from n ≥ 5 independent experiments. *P < 0.05; **P < 0.01 (One-way ANOVA Dunnett's multiple comparison). (f and g) Representative FACS plots of sorted hybrids using D1 (natural control) medium (f) or D7 (natural damage) medium (g) gating the GFP+RFP+ with 4n or higher ploidy (orange squares). (h) FACS data quantification of GFP+RFP+ 4n hybrids obtained with D1 or D7 media, with or without Chiron-mediated Wnt/beta-catenin pathway activation of the AD-hMSC. Data are presented as individual values, mean ± SEM from n ≥ 2 independent experiments.

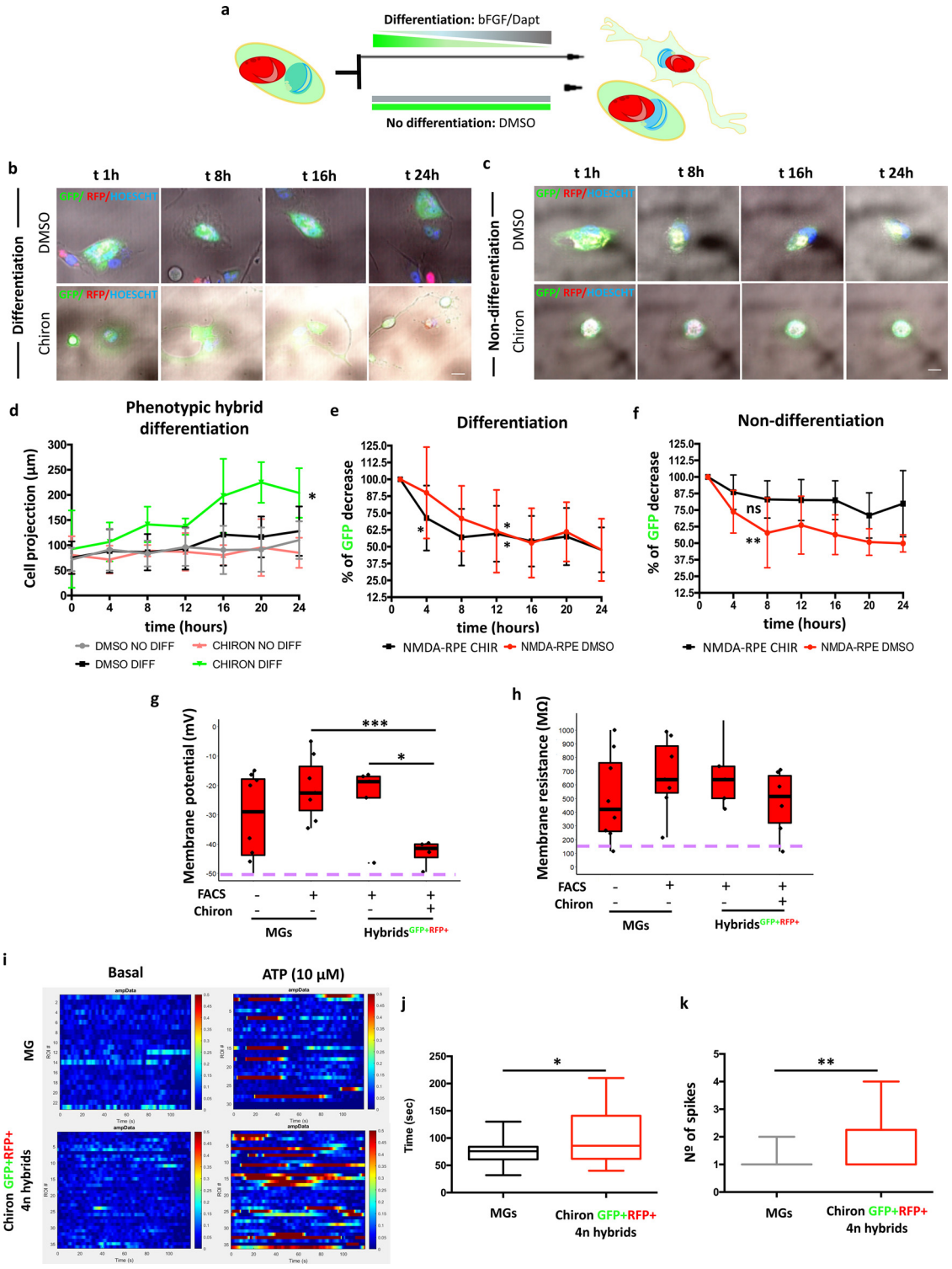

Figure 3. GFP+RFP+ 4n hybrids can differentiate toward a neural-like lineage and show electrophysiological properties. (a) Experimental scheme showing GFP+RFP+ 4n hybrids differentiation into a neural-like phenotype when cultured in the presence of hFGF2 and the NOTCH inhibitor (DAPT) for 24h (Differentiation) and the lack of differentiation when using DMSO as control (No differentiation). (b and c) Representative snapshots of time lapse imaging of GFP+RFP+ 4n hybrids resulting from the fusion of MG^{GFP} with $AD\text{-}hMSC^{RFP}$, generated in the presence of NMDA-RPE medium, with or without Chiron-treatment of the AD-hMSC, and cultured in

hybrids obtained from AD-hMSCs that were not Wnt/beta-catenin activated and the FACS-sorted MG that were and cultured in differentiation medium (Figure 3g). The -45mV value is comparable to the ganglion cell resting membrane potential.[51,52] In contrast, the hybrids that had not been cultured in differentiation medium, irrespective of the Wnt/beta-catenin pathway activation in the AD-hMSCs, exhibited higher resting potential as compared with the differentiated ones (Figure S4b). However, the membrane resistance did not significantly differ between groups (Figure 3h), likely suggesting that the hybrids did not acquire mature electrophysiological properties. In conclusion, the electro-profile of the hybrids obtained from AD-hMSC treated with Chiron and cultured in NMDA-RPE medium suggests that these cells can initiate a differentiation process toward a neuronal phenotype.[53,54]

To further characterize the hybrids obtained from the fusion of AD-hMSCs treated with Chiron and cultured in NMDA-RPE medium (Chiron GFP+RFP+ 4n hybrids) we assessed their electrophysiological population properties. To do so, we performed Fluo4-AM calcium imaging of the FACS-sorted MG, as a control, (supplementary video 9) and of the hybrids (supplementary video 10) after two days of differentiation. We measured the basal activity and their response to 10 micromolar ATP activation for 2 min (Figure 3i). While basal activity was virtually inexistent in both FACS-sorted MG and Chiron GFP+RFP+ 4n hybrids, both of them responded to the ATP activation. Although they showed different heat map profiles, the amplitude of the signal was not significantly different between the two cell types (Figure S4c), suggesting that both FACS-sorted MG and the hybrids are able to intake ATP up to a similar maximum amplitude. However, when we analyzed the average time of cell activation by measuring the time that the imaged cells were active (with an amplitude > 0,25), we found that the hybrids were significantly more active over time, suggesting they could keep their channels open for longer (Figure 3j). Moreover, we investigated whether the channels were open continuously or in spikes, by measuring the number of spikes (activation of > 10 seconds)[55] in a 2-minute imaging. Interestingly, while FACS-sorted MG predominantly showed just one broad spike, the hybrids' response was significantly different, since they could intake ATP in multiple spikes (Figure 3k). These results confirm the electrophysiological properties of the Chiron GFP+RFP+ 4n hybrids upon neural differentiation.

Hybrid integration and differentiation can be observed in maturing human retinal organoids

To investigate the potential of the hybrids to differentiate toward a ganglion-like phenotype *in vivo*, we modeled *in vivo* conditions by transplanting hybrids into retinal organoids generated from hESCs. The differentiation conditions we used promoted the formation of islet-like structures comprising small spheres of neural precursor cells in 2D cultures. From day 15 onwards, 3D structures started to emerge, and from day 30 onwards lamination of the cells was identified. Subsequently, they self-organized into optic cup-like structures with small invaginations (day 42) (Figure S4d). These results agreed with previous reports.[56] In order to identify the optimal time for micro-injection, the organoids were fixed, sectioned and immunostained for the ganglion specific marker B-III TUBULIN (red) and the glial family marker GS (green), at four different time points (day 35, 40, 45, and 50). After quantifying GS+ and B-III TUBULIN+ cells, we observed comparable numbers of GS+ cells at all time points analyzed, while the number of B-III TUBULIN+ cells increased significantly by day 40 (Figure 4a-c). Moreover, at day 40 all B-III TUBULIN+ cells were found in the inner part of the organoid (yellow asterisk) (Figure 4a). Taken together, we concluded that day 40 was the optimal time point to perform the micro-injection of the hybrids.

differentiation (b) or non-differentiation (c) medium. GFP is expressed from the pRLBP of MG^{GFP}, and RFP from AD-$hMSC^{RFP}$. Scale bar = 50 μm. (d) Measurement of the projection length in hybrids generated as described in b and c, and cultured in differentiation or non-differentiation media. Data are presented as grouped values, mean ± SEM from n ≥ 4 independent cells from n ≥ 2 independent experiments. ns = non-significant; *P < 0.05 (One-way ANOVA Tukey's multiple comparison). (e and f) Percentage of decrease in GFP fluorescent intensity, measured in hybrids generated as described in b and c and cultured in differentiation (e) or non-differentiation (f) media. Data are presented as grouped values, mean ± SEM from n ≥ 3 independent experiments. ns = non-significant; *P< 0.05; **P < 0.01 (Two-way ANOVA Tukey's multiple comparison). (g) Resting membrane potential measured in MG and in hybrids generated as described in b and c, before and after FACS-sorting, and cultured in differentiation medium. (h) Membrane resistance measured in MG and in hybrids generated as described in b and c, before and after FACS-sorting, and cultured in differentiation medium. (g and h) Data are presented as grouped values, mean ± SEM from n ≥ 3 independent experiments. ns = non-significant; *P < 0.05; **P < 0.01; ***P < 0.001 (Two-way ANOVA Tukey's multiple comparison). (i) Heat map of FACS-sorted MG (MG, upper row) and hybrids obtained from AD-hMSC treated with Chiron (Chiron GFP+RFP+ 4n Hybrids) generated as described in b (Chiron, lower row) in basal conditions (left column) or 10 micromolar ATP activation (right column). Data is presented as single values from n ≥ 10 cells. (j) ATP-intake response time of MG and hybrids (Chiron GFP+RFP+ 4n Hybrids), after ATP stimulation. Data is presented as grouped values from n ≥ 8. *P < 0.05 (Unpaired t-test with Welch's correction). (k) Number of ATP intake spikes for MG and hybrids (Chiron GFP+RFP+ 4n Hybrids), after ATP stimulation. Data is presented as grouped values from n ≥ 8. **P < 0.01 (Unpaired t-test with Welch's correction).

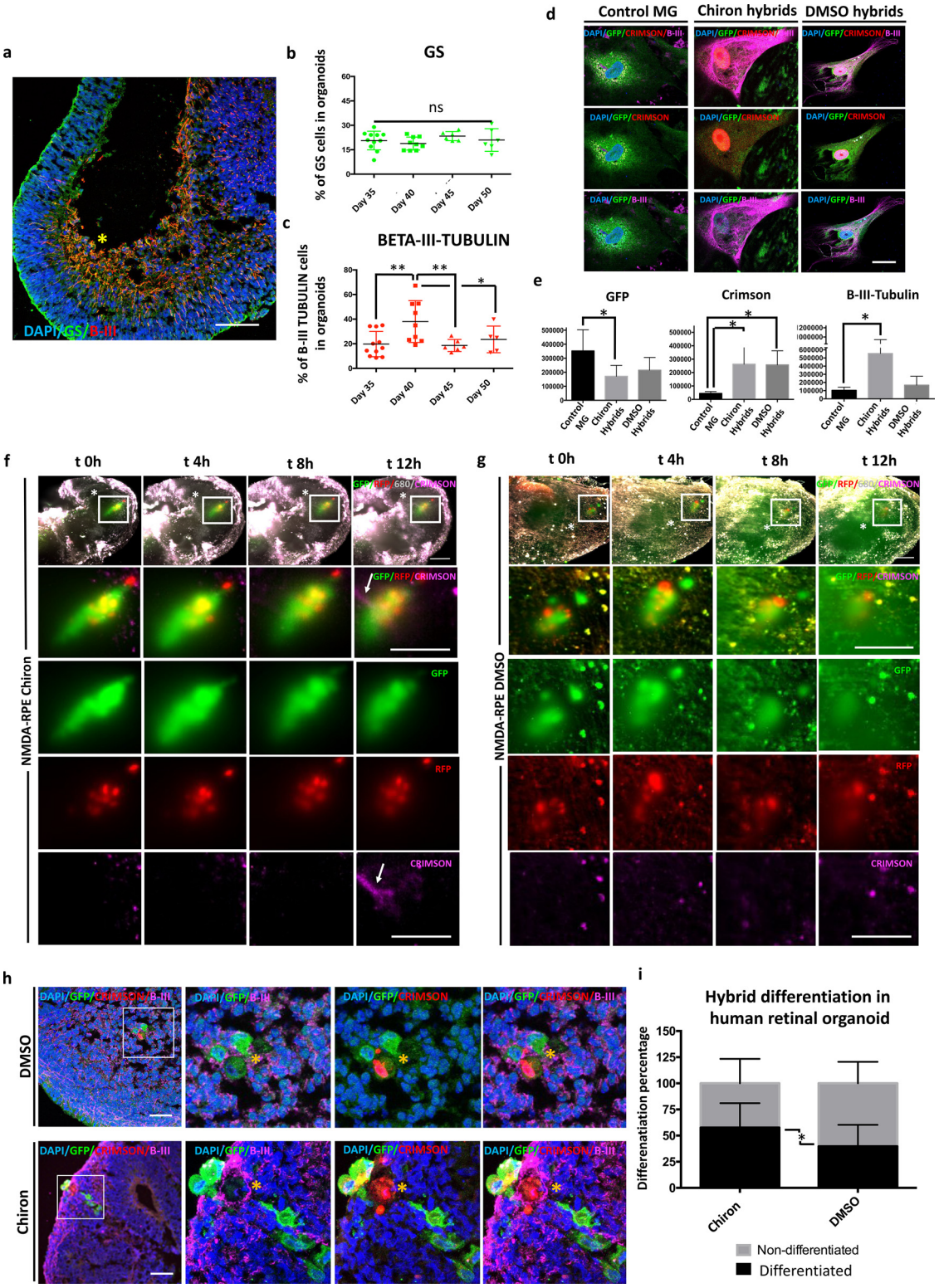

Figure 4. GFP+RFP+ 4n hybrids generated with Wnt/beta-catenin–activated AD-hMSCs can integrate within the human retinal organoids and differentiate toward a neural fate. (a) Immunostaining using antibodies against B-III TUBULIN (red) or GS (green) in a section of human retinal organoids. Representative image of organoid at day 40. Scale bar = 100 μm. (b and c) Quantification of MG

We then engineered the MG^{GFP} by introducing the fluorescence protein CRIMSON, under the expression of the neuronal specific promoter *TUJ1*, to generate MG-*pRLBP*_eGFP_*TUJ1*_CRIMSON (herein, $MG^{GFP/CRIMSON}$). FACS analysis and quantification of MG $^{GFP/CRIMSON}$ cultured in differentiation medium (20 ng/ml hFGF2 and 50 μM DAPT), showed a minor increase of CRIMSON expression at 24 and 48h of differentiation (Figure S4e − S4g). Still, as proved by the patch clamp experiment, MG cultured in differentiation medium do not acquire neural electrophysiological features (Figure 3g and 3h). We then generated the hybrids by fusing $MG^{GFP/CRIMSON}$ with AD-$hMSC^{H2B:mRFP}$ treated with Chiron or DMSO, and cultured the cells in NMDA-RPE medium. Sorted hybrids were then differentiated for 48 h and immunostained to assess their *in vitro* differentiation. While MG in control conditions did not appear differentiated, GFP+RFP+ 4n hybrids generated from Chiron-activated AD-$hMSC^{H2B:mRFP}$ showed a decreased GFP signal in the cytoplasm and a corresponding increased CRIMSON intensity co-localized with B-III TUBULIN as shown in Figure 4d) and quantified in Figure 4e, suggesting the differentiation of the hybrids towards a neural fate.

Having established the differentiation potential and electrophysiological properties of the hybrids *in vitro*, we concluded that hybrids resultant from the fusion of Chiron-treated AD-$hMSC^{H2B:mRFP}$ have the greatest potential for neural-like differentiation. We then aimed to inject these GFP+RFP+ 4n hybrids into the retinal organoids to follow their differentiation, along with the intrinsic ganglion cell development within the organoid. We first established a new procedure, adapting an embryo micro-injection technique for the organoids, and, using this procedure, injected 20−25 GFP+RFP+ 4n hybrids ($MG^{GFP/CRIMSON}$ fused with AD-$hMSC^{H2B:mRFP}$) into the retina. The injection was targeted to the laminated part of the organoid, which was held with a micro-pipette (Figure S4h and i). Based on the previous observations, we hypothesized that the hybrids generated in the presence of pro-inflammatory molecules had a greater potential to integrate in the organoids, lose the MG features and differentiate. We therefore injected GFP+RFP+ 4n hybrids, generated with AD-$hMSC^{H2B:mRFP}$ treated or not with Chiron and cultured with NMDA-RPE medium (Figure 4f, g). Once injected, the organoids were imaged for 12 h. Over time, we observed a decrease of GFP intensity (from the *pRLBP* promoter) in the hybrids generated with Chiron-treated AD-$hMSC^{H2B:mRFP}$ and cultured in NMDA-RPE medium, while the RFP signal (from the $hMSC^{H2B:mRFP}$) poorly diminished. Interestingly, from 8h to 12h, we distinguished faint expression of CRIMSON only in the hybrids formed by $MG^{GFP/CRIMSON}$ fused with Chiron-treated AD-$hMSC^{H2B:mRFP}$ (CRIMSON expressed from the *TUJ1* promoter, white arrows) and cultured in the NMDA-RPE medium (Figure 4f).

To confirm the differentiation potential of the injected hybrids toward a ganglion phenotype, the microinjected organoids were fixed and sectioned after 24 h and processed for immunostaining against GFP, CRIMSON and the ganglion marker B-III TUBULIN (Figure 4h). While the control hybrids (generated from fusion of AD-$hMSC^{H2B:mRFP}$ treated with DMSO) appeared as clumps in the injection point, the hybrids generated from fusion of AD-$hMSC^{H2B:mRFP}$ treated with Chiron were dispersed away from the injection site and intermixed among the host cells, suggesting integration into the tissue. Additionally, they were clearly differentiated, expressing a dim or almost inexistent GFP signal (orange asterisk), while there was a clear CRIMSON signal (red) colocalizing with the ganglion cell marker b-III- TUBULIN (magenta) (Figure 4h, lower row). The control hybrids showed spotty and a dimmer, almost non-detectable CRIMSON (Figure 4h, red, upper row) that co-localized with a bright GFP signal (green, orange asterisk) but did not co-localize with the B-III TUBULIN signal (Figure 4h magenta, upper row). The quantification of the hybrids displaying dim GFP while positive for CRIMSON and B-III TUBULIN

(Glutamine synthetase, GS, green) (b) and ganglion cell (B-III TUBULIN, B-III, red) (c) numbers normalized by the total DAPI (blue) cells in growing organoids from day 35 to day 50 of differentiation. Data are presented as individual values, mean ± SEM from n ≥ 3 independent experiments (quantifying at least 3 random fields per time point and experiment). ns = non-significant; *P < 0.05; **P < 0.01 (One-way ANOVA Dunnett's multiple comparison). (d and e) Representative immunostaining (d) and intensity quantification (e) of MG and of hybrids ($MG^{GFP/CRIMSON}$ fused with AD-$hMSC^{H2B:mRFP}$) generated in the presence of NMDA-RPE medium, using AD-$hMSC^{H2B:mRFP}$ treated or not with Chiron. Cells were cultured in differentiation medium. GFP (green) is expressed from the pRLBP of $MG^{GFP/CRIMSON}$ and CRIMSON (red) from the TUJ1 promoter. The B-III TUBULIN neural marker is shown in magenta. Data are presented as individual values, mean ± SEM from n ≥ 3 hybrid cells. (f and g) Representative snapshot of live cell imaging max-projection of growing organoids micro-injected with hybrids generated as described in e. AD-$hMSC^{H2B:mRFP}$ were treated with Chiron (f) or with DMSO (g). Lower panels show a 3 × zoom-in of the injected hybrids. Cells on the organoid surface were labelled by VivoTrack 680. Zoomed images of the injected hybrids were split in the three-color channels. (h) Immunostaining of human retinal growing organoids microinjected with hybrids generated as described in e. Representative experimental images are shown. Immunostaining with antibodies against GFP (encoded from pRLBP of $MG^{GFP/CRIMSON}$, in green), CRIMSON (encoded from TUJ1 promoter of $MG^{GFP/CRIMSON}$, in red) or the B-III TUBULIN neural marker (magenta). (i) Percentage of differentiated hybrids showing a neuronal phenotype, determined by quantifying CRIMSON-positive cells (from TUJ1 expression) that colocalized with B-III TUBULIN (magenta) and GFP (encoded from pRLBP of the $MGs^{GFP/CRIMSON}$). Data are presented as grouped values, mean ± SEM from n ≥ 3 organoids per condition. *P < 0.05 (One-way ANOVA Dunnett's multiple comparison).

expression, which thus showed ganglion cell fate within the growing organoids, demonstrated their significant differentiation potential. Specifically, within the organoids, we found a higher percentage of differentiated hybrids when microinjecting the hybrids generated with AD-hMSC$^{H2B:mRFP}$ treated with Chiron (57%) as compared to the injection of the control hybrids (39%) (Figure 4i).

Discussion

In this work, we found that MG can fuse with adult stem cells in human retina *ex vivo*. By studying the fusion process *in vitro*, we demonstrated that cell-fusion efficiency increases when cells are exposed to molecules secreted by injured cells. Moreover, hybrids generated in the presence of the NMDA-RPE medium showed enhanced ability to differentiate into neural-like cells. Differentiation is faster and is increased when the Wnt/beta-catenin pathway is activated in the adult stem cells used for the fusion. Finally, we established an experimental system to investigate hybrid viability within growing retinal tissue using retinal organoids and a micro-injection protocol for transplanting them. This allowed us to assess that the hybrids present engraftment and differentiation potential, which can be used in the future for *in vivo* applications.

Cell fusion is recognized as a possible mechanism contributing to tissue regeneration. In fact, even if rare, cell fusion events have been consistently detected in human tissues, including the liver, brain, and gastrointestinal tract, often in post-mortem analysis.[57-59] In the studies reported here, we identified cell-fusion events in the human retina. In the experiments performed using organotypic cultures, the physiological autolysis might also have created an injury response, facilitating fusion. Similarly, in many retinopathies, neuron degeneration might create an environment that facilitates fusion of transplanted cells.[57-59]

Our observations regarding the potential of hybrids to undergo differentiation towards neural-like precursors are in accordance with previously published data on retinal progenitor cells that undergo differentiation towards neural fate when cultured with bone marrow–derived medium enriched with different growth factors. These culture conditions promote differentiation of retinal progenitors into a neural lineage and offer neural protection upon *in vivo* engraftment.[5,60-62]

Fusion of MSCs and MG is enhanced by the natural damage occuring within an old organotypic retinal culture or by NMDA-mediated chemical damage. Moreover, this spontaneous cell fusion is independent of the type of adult stem cells used. Interestingly, it has been previously shown that co-transplantation of hMSCs and human bone marrow–derived cells leads to an increased regenerative effect, with engraftment resulting in more than a two-fold increase of chimerism as compared to a single-cell type transplant.[63] In a mouse model of type 1 diabetes, homing of HSPCs to the pancreas increased when HSPCs were co-transplanted intravenously with MSCs.[64] It will be interesting to determine whether in these co-transplantation experiments, the enhanced regeneration also resulted from fusion events.

MSCs were shown to have a supportive effect on the HSPC cultures, via the release of HIF-1alpha.[65] Considering the Wnt/beta-catenin role in enhancing reprogramming, together with the previously described role of YAP in controlling MG proliferation,[66,67] we can postulate that a time-refined crosstalk in a pro-inflammatory context could stimulate the regenerative capabilities of dormant MG to favor retina regeneration. On the other hand, these aspects are difficult to be studied in vitro, since the autolytic changes in the experiments performed with retinal explants might have altered the signaling pathway activities.

In mice, previous studies demonstrated the potential of the hybrids generated *in vivo* to be reprogrammed and differentiate towards retinal ganglion cells, as well as their ability to contribute to the optic nerve regeneration and to photoreceptor regeneration, leading to a functional rescue.[21,22] Due to the limitations of our human model systems, which did not allow us to isolate enough hybrids to perform an exhaustive analysis, we could not investigate whether the human hybrids were reprogrammed upon Wnt-activation. However, similarly to what was found in mice, we observed that the human hybrids had lost MG identity and could differentiate toward ganglion cell fates, exhibiting a neural-like phenotype, including the polarization of the soma, the formation of podocyte-like structures, and the acquisition of neuron-like electrical properties. However, the membrane resistance values of the hybrids were not comparable to neuronal ones, probably because expression of ion-channels, such as the voltage-gated Na^+ channel, is still not present 24h after differentiation. As such, no action potentials were observed upon the injection of depolarizing current pulses.[68] ATP is known to stimulate both ganglion cells[69] and glial cells.[70] Interestingly, after ATP stimulation, we observed that the hybrids, unlike MG, had neural-like electrical features, which were sustained in time, and spike distribution of intake, further confirming differentiation toward a neural phenotype. Increased differentiation might be assessed in the future not only by analyzing the voltage channels after ATP stimulation, but also by measuring the response of Cannabinoid, P2 × 7 or glycine receptors.[71,72]

Even if we observed neural electrophysiological features, the expression of the pan-neuronal marker TUJ1 together with the development of a stable resting membrane potential and soma polarization suggest that the differentiation towards a neuronal phenotype has initiated, but is not yet completed after 48h. Glycosylation

levels can change in the neural stem cells along with the fate conversion, and glycosylation can prime the astroglia towards a ganglion cell fate.[73] Thus, it will be interesting in the future to study whether the glycosylation modifications in the MG could promote even more the differentiation process after fusion.

Lastly, we studied how hybrids differentiate in a living tissue. Because retina organotypic cultures degenerate already after one week of culture, we decided to use human retinal organoids.[25,56,74] Interestingly, growing organoids have been found to recapitulate human retinal development and cellular organization.[75] Additionally, retinal organoids form functional synapses and show light responses. When comparing retinal organoid development with embryonic retinogenesis (between 7 and 20 weeks) at single-cell transcriptome level [48, 64-66], negligible differences were found. These results showed that "mature" organoids resemble human retinae, and neural development within the organoids proceeds in accordance with a natural neurogenesis.[76] Thus, organoids open a broad number of possibilities – that could be combined with the newest technologies, such as single-cell sequencing or single-cell multi-omics – to, for example, study neural development and the origin of visual disorders.[77] We utilized growing organoids as a host tissue for engrafting hybrids as a mean to study the hybrids' interactions within a living tissue and their differentiation potential. We propose a new use for human retinal organoids as a model for stem cell-based retinal regeneration. For example, this will allow us to also study the migration and integration of transplanted cells after the adult stem cells are chemoattracted to the tissue.[24] Additionally, in a functional organoid, the electrophysiology potential of differentiated cells could be tested in an *in vivo* human model. This can be further combined with new technologies, such as mesoscopic microscopy for longer *in vivo* imaging, the CRISPR/CAS9 technology to generate visual impaired organoids, and the adaptation of cell-tracer techniques, including brainbow.[78,79] These methods would allow the human retina interconnections and the differentiation of the micro-injected hybrids to be studied, going one step further in the investigation of human retinal regeneration.

Our approach to using hybrid-mediated regenerative therapy as a future prospect for treatment goes hand-in-hand with other approaches that focus on regenerating the human retina using a number of different stem-cell types. For instance, some studies have reported the possibility of developing *in vitro* differentiated retinal cell types, such as the retinal ganglion cells or photoreceptors, for subsequent transplantation into the damaged retina.[80,81] Another approach is the use of scaffolds to grow monolayers of differentiated cells, in order to transplant the full retinal sheet, thereby ensuring proper positioning of the cells in the eye environment.[82,83] Additionally, it is important to highlight that although the stem cells that we use in this study can engraft in the retinal tissue, most of them do not fuse with resident cells. Previous studies demonstrated that entosis is an alternative process, whereby differentiated cells are engulfed by the stem cells, without nuclear fusion.[30] Thus, cell entosis could be an additional mechanism to eliminate those cells that cannot be rescued.

Importantly, even if the adult stem cells will be transplanted into the subretinal or intravitreal space of patients, this does not mean that they will be in close contact with the damaged tissue. Hence, these stem cells must be attracted to the damaged area in order to heal it. Specific chemokines are over-expressed during retinal damage and can attract MSCs. Following overexpression of the chemokine receptors Ccr5 and Cxcr6 in mouse MSCs, improved cell migration and integration into a damaged mouse retina were observed. The integrated cells could trans-differentiate and enhance retinal rescue.[24] A similar approach should be considered for human adult stem cell transplantation attempts in order to enhance the regenerative process in patients.

Lastly, one of the most important points to investigate about the hybrids is the possibility of ploidy reduction. After fusion, hybrids are tetraploid, which might potentially lead to chromosomal instability and cancer development.[84,85] On the other hand, as we described here, cell fusion and tetraploid hybrids can potentially contribute to tissue rescue and regeneration. Hence, we hypothesize that there might be tightly regulated ploidy reduction to avoid chromosome mis-segregation and cancer development. Previous work showed that tetraploid hybrids that were injected into blastocysts can undergo ploidy reduction upon tripolar mitosis, with random and non-random chromosome segregation, resulting in diploid cells that contributed to the adult tissues in chimeric mice.[47] Notably, in the case of the liver, tetraploid hepatocytes can act as a genetic reservoir able to undergo reductive mitosis in response to stress and injury.[86] Therefore, a similar mechanism might occur also for the 4n retinal hybrids during retinal regeneration.

In conclusion, our results indicate that the hybrids between MG and adult stem cells might be a promising stem cell–mediated therapy for human retina rescue and, potentially, for its regeneration. However, much work remains to be done to develop an efficient therapy to treat visual impairment via cell fusion approaches.

Contributors

S.A.B-P. and M.P.C. conceived and designed the study. S.A.B-P., M.P., S.N., E.G.B., A.F-B., D.G., and E.D-S. performed experiments. J.C.D'A. and R.I.B. provided help with the human retinae experiments. R.S-P. help with cloning design. A.F-B. and M.D. devised, carries out and analyzed Ephys experiments. R.G-R. wrote the imaging analysis script. S.A.B-P. analyzed data. N.M.P.

help in the organoid experiments and data supervision. M.D.S help in the electrophysiology data supervision. M.P.C. and S.A.B-P. wrote the manuscript and verified the data. M.P.C. supervised the project. All authors read and approved the final version of the manuscript.

Funders

This work was supported by La Caixa Health (HR17-00231 to M.P.C., N.M. and J.C.D'A.), by Velux Stiftung (976a to M.P.C.), the Ministerio de Ciencia e Innovación, (BFU2017-86760-P to M.P.C.) (AEI/FEDER, UE), the AGAUR grant from Secretaria d'Universitats i Recerca del Departament d'Empresa i Coneixement de la Generalitat de Catalunya, (2017 SGR 689 to M.P.C. and 2017 SGR 926), the European Union's Horizon 2020 research and innovation program (grant agreement N°964342 to M.P.C); the subprograma estatal de Formación del Ministerio de Economía y Competitividad ref. BES-2015-075805 (to S. A.B-P.) and ref. BES-2015-075802 (to M.P.), the Secretaria d'Universitats i Recerca del Departament d'Empresa i Coneixement de la Generalitat de Catalunya ref. 2018FI_B_00637 (to R.S.-P.), and the co−finance of Fondo Social Europeo (FSE to R.S.-P.). We also acknowledge the support of the Agencia Estatal de Investigación (PID2019-110755RB-I00/AEI / 10.13039/501100011033), JPND Heroes Ministerio de Ciencia Innovación y Universidades (RTC2019-007230-1 and RTC2019-007329-1) and NIH (Grant Number: 1R01EB 028159-01) to MD. The lab of MD also acknowledges the support of the Agencia Estatal de Investigación (PID2019-110755RB-I00/AEI / 10.13039/501100011033). We acknowledge support of the Spanish Ministry of Science and Innovation to the EMBL partnership, the Centro de Excelencia Severo Ochoa and the CERCA Programme / Generalitat de Catalunya. The CIBER of Rare Diseases is an initiative of the ISCIII.

Data Sharing Statement

All the data supporting our findings are available upon request. The data are not publicly available due to ethical restrictions.

Declaration of interests

M.P.C. declares her interest as follows: Grants from Velux Stiftung, Ministerio de Ciencia e Innovación, AGAUR, Agencia Estatal de Investigación, European Union's Horizon 2020 research and innovation program (grant agreement N° 964342). M.P.C. and S.A.B-P. declare their interest in the grant Subprograma estatal de Formación del Ministerio de Economía y Competitividad ref.BES-2015-075805. M.P.C. and M.P. declare their interest in the grant Subprograma estatal de Formación del Ministerio de Economía y Competitividad ref. BES-2015-075802. M.P.C. and R.S-P. declare their interest in the grant Secretaria d'Universitats i Recerca del Departament d'Empresa i Coneixement de la Generalitat de Catalunya and the co−finance of Fondo Social Europeo. M.P.C., N.M., R.I.B. and J.C.D'A. declare their interest in the grant La Caixa Health (HR17-00231). M. D. declare her interest in AGAUR 2017 SGR 926 & Agencia Estatal de Investigación (PID2019-110755RB-I00/AEI / 10.13039/501100011033). M.P.C., N.M. and E.G.B. declare the participation of IBEC in the human retina organoids production and characterization. M.P. C. declare the participation of Centre d'Oftalmologia Barraquer & Institut Universitari Barraquer as the human eye globe providers. All other authors declare no competing interest.

Acknowledgments

We thank Prof. Peter F. Hitchcock for his precious and critical suggestions on the content and style of the manuscript. We also thank the UPF/CRG Flow Cytometry Unit and the CRG Advanced Light Microscopy Unit for their support in this work.

Supplementary materials

Supplementary material associated with this article can be found in the online version at doi:10.1016/j.ebiom.2022.103914.

References

1 Goldman D. Muller glial cell reprogramming and retina regeneration. *Nat Rev Neurosci*. 2014;15(7):431–442.
2 Blackshaw S, Harpavat S, Trimarchi J, et al. Genomic analysis of mouse retinal development. *PLoS Biol*. 2004;2(9):E247.
3 Dyer MA, Cepko CL. Control of Muller glial cell proliferation and activation following retinal injury. *Nat Neurosci*. 2000;3(9):873–880.
4 Vetter ML, Hitchcock PF. Report on the national eye institute audacious goals initiative: replacement of retinal ganglion cells from endogenous cell sources. *Transl Vis Sci Technol*. 2017;6(2):5.
5 Mead B, Chamling X, Zack DJ, Ahmed Z, Tomarev S. TNFalpha-mediated priming of mesenchymal stem cells enhances their neuroprotective effect on retinal ganglion cells. *Invest Ophthalmol Vis Sci*. 2020;61(2):6.
6 Usategui-Martin R, Puertas-Neyra K, Garcia-Gutierrez MT, Fuentes M, Pastor JC, Fernandez-Bueno I. Human mesenchymal stem cell secretome exhibits a neuroprotective effect over *in vitro* retinal photoreceptor degeneration. *Mol Ther Methods Clin Dev*. 2020;17:1155–1166.
7 George S, Hamblin MR, Abrahamse H. Differentiation of mesenchymal stem cells to neuroglia: in the context of cell signalling. *Stem Cell Rev Rep*. 2019;15(6):814–826.
8 Mahmoudian-Sani MR, Forouzanfar F, Asgharzade S, Ghorbani N. Overexpression of MiR-183/96/182 triggers retina-like fate in human bone marrow-derived mesenchymal stem cells (hBMSCs) in culture. *J Ophthalmol*. 2019;2019: 2454362.
9 Nitobe Y, Nagaoki T, Kumagai G, et al. Neurotrophic factor secretion and neural differentiation potential of multilineage-differentiating stress-enduring (Muse) cells derived from mouse adipose tissue. *Cell Transplant*. 2019;28(9−10):1132–1139.
10 Helbling PM, Pineiro-Yanez E, Gerosa R, et al. Global transcriptomic profiling of the bone marrow stromal microenvironment during postnatal development, aging, and inflammation. *Cell Rep*. 2019;29(10):3313–3330. e4.

11 Lee SG, Moon SH, Kim HJ, et al. Bone marrow-derived progenitor cells in de novo liver regeneration in liver transplant. *Liver Transpl*. 2015;21(9):1186–1194.
12 Meyer MB, Benkusky NA, Sen B, Rubin J, Pike JW. Epigenetic plasticity drives adipogenic and osteogenic differentiation of marrow-derived mesenchymal stem cells. *J Biol Chem*. 2016;291 (34):17829–17847.
13 Shi H, Li X, Yang J, et al. Bone marrow-derived neural crest precursors improve nerve defect repair partially through secreted trophic factors. *Stem Cell Res Ther*. 2019;10(1):397.
14 Pedone E, Olteanu VA, Marucci L, et al. Modeling dynamics and function of bone marrow cells in mouse liver regeneration. *Cell Rep*. 2017;18(1):107–121.
15 Benigni A, Morigi M, Remuzzi G. Kidney regeneration. *Lancet*. 2010;375(9722):1310–1317.
16 Loffredo FS, Steinhauser ML, Gannon J, Lee RT. Bone marrow-derived cell therapy stimulates endogenous cardiomyocyte progenitors and promotes cardiac repair. *Cell Stem Cell*. 2011;8(4):389–398.
17 Nygren JM, Jovinge S, Breitbach M, et al. Bone marrow-derived hematopoietic cells generate cardiomyocytes at a low frequency through cell fusion, but not transdifferentiation. *Nat Med*. 2004;10 (5):494–501.
18 Pesaresi M, Bonilla-Pons SA, Simonte G, Sanges D, Di Vicino U, Cosma MP. Endogenous mobilization of bone-marrow cells into the murine retina induces fusion-mediated reprogramming of Muller glia cells. *EBioMedicine*. 2018;30:38–51.
19 Lluis F, Pedone E, Pepe S, Cosma MP. Periodic activation of Wnt/beta-catenin signaling enhances somatic cell reprogramming mediated by cell fusion. *Cell Stem Cell*. 2008;3(5):493–507.
20 Sanges D, Lluis F, Cosma MP. Cell-fusion-mediated reprogramming: pluripotency or transdifferentiation? Implications for regenerative medicine. *Adv Exp Med Biol*. 2011;713:137–159.
21 Sanges D, Romo N, Simonte G, et al. Wnt/beta-catenin signaling triggers neuron reprogramming and regeneration in the mouse retina. *Cell Rep*. 2013;4(2):271–286.
22 Sanges D, Simonte G, Di Vicino U, et al. Reprogramming Muller glia via in vivo cell fusion regenerates murine photoreceptors. *J Clin Invest*. 2016;126(8):3104–3116.
23 Pesaresi M, Sebastian-Perez R, Cosma MP. Dedifferentiation, transdifferentiation and cell fusion: in vivo reprogramming strategies for regenerative medicine. *FEBS J*. 2019;286(6):1074–1093.
24 Pesaresi M, Bonilla-Pons SA, Sebastian-Perez R, et al. The chemokine receptors Ccr5 and Cxcr6 enhance migration of mesenchymal stem cells into the degenerating retina. *Mol Ther*. 2020.
25 Eiraku M, Sasai Y. Mouse embryonic stem cell culture for generation of three-dimensional retinal and cortical tissues. *Nat Protoc*. 2011;7(1):69–79.
26 McQuin C, Goodman A, Chernyshev V, et al. CellProfiler 3.0: next-generation image processing for biology. *PLoS Biol*. 2018;16:(7) e2005970.
27 Pellissier LP, Hoek RM, Vos RM, et al. Specific tools for targeting and expression in Muller glial cells. *Mol Ther Methods Clin Dev*. 2014;1:14009.
28 Piedra J, Ontiveros M, Miravet S, Penalva C, Monfar M, Chillon M. Development of a rapid, robust, and universal picogreen-based method to titer adeno-associated vectors. *Hum Gene Ther Methods*. 2015;26(1):35–42.
29 Singhal S, Bhatia B, Jayaram H, et al. Human Muller glia with stem cell characteristics differentiate into retinal ganglion cell (RGC) precursors in vitro and partially restore RGC function in vivo following transplantation. *Stem Cells Transl Med*. 2012;1 (3):188–199.
30 Sottile F, Aulicino F, Theka I, Cosma MP. Mesenchymal stem cells generate distinct functional hybrids in vitro via cell fusion or entosis. *Sci Rep*. 2016;6:36863.
31 Mederos S, Sanchez-Puelles C, Esparza J, Valero M, Ponomarenko A, Perea G. GABAergic signaling to astrocytes in the prefrontal cortex sustains goal-directed behaviors. *Nat Neurosci*. 2021;24(1):82–92.
32 Arganda-Carreras I, Fernandez-Gonzalez R, Munoz-Barrutia A, Ortiz-De-Solorzano C. 3D reconstruction of histological sections: application to mammary gland tissue. *Microsc Res Tech*. 2010;73 (11):1019–1029.
33 Schindelin J, Arganda-Carreras I, Frise E, et al. Fiji: an open-source platform for biological-image analysis. *Nat Methods*. 2012;9 (7):676–682.
34 de Witte SFH, Luk F, Sierra Parraga JM, et al. Immunomodulation by therapeutic Mesenchymal Stromal Cells (MSC) is triggered through phagocytosis of MSC by monocytic cells. *Stem Cells*. 2018;36(4):602–615.
35 Niyadurupola N, Sidaway P, Osborne A, Broadway DC, Sanderson J. The development of Human Organotypic Retinal Cultures (HORCs) to study retinal neurodegeneration. *Br J Ophthalmol*. 2011;95(5):720–726.
36 Bennett J, Wellman J, Marshall KA, et al. Safety and durability of effect of contralateral-eye administration of AAV2 gene therapy in patients with childhood-onset blindness caused by RPE65 mutations: a follow-on phase 1 trial. *Lancet*. 2016;388(10045):661–672.
37 Tolmachova T, Tolmachov OE, Barnard AR, et al. Functional expression of Rab escort protein 1 following AAV2-mediated gene delivery in the retina of choroideremia mice and human cells ex vivo. *J Mol Med (Berl)*. 2013;91(7):825–837.
38 Bland JM, Altman DG. Statistics notes. The odds ratio. *BMJ*. 2000;320(7247):1468.
39 Limb GA, Salt TE, Munro PM, Moss SE, Khaw PT. In vitro characterization of a spontaneously immortalized human Muller cell line (MIO-M1). *Invest Ophthalmol Vis Sci*. 2002;43(3):864–869.
40 Ring DB, Johnson KW, Henriksen EJ, et al. Selective glycogen synthase kinase 3 inhibitors potentiate insulin activation of glucose transport and utilization in vitro and in vivo. *Diabetes*. 2003;52 (3):588–595.
41 Nusse R, Clevers H. Wnt/beta-catenin signaling, disease, and emerging therapeutic modalities. *Cell*. 2017;169(6):985–999.
42 Dominici M, Le Blanc K, Mueller I, et al. Minimal criteria for defining multipotent mesenchymal stromal cells. The international society for cellular therapy position statement. *Cytotherapy*. 2006;8 (4):315–317.
43 Mushahary D, Spittler A, Kasper C, Weber V, Charwat V. Isolation, cultivation, and characterization of human mesenchymal stem cells. *Cytometry A*. 2018;93(1):19–31.
44 Ola MS, Moore P, El-Sherbeny A, et al. Expression pattern of sigma receptor 1 mRNA and protein in mammalian retina. *Brain Res Mol Brain Res*. 2001;95(1–2):86–95.
45 Reigada D, Lu W, Mitchell CH. Glutamate acts at NMDA receptors on fresh bovine and on cultured human retinal pigment epithelial cells to trigger release of ATP. *J Physiol*. 2006;575(Pt 3):707–720.
46 Kim J, Sajid MS, Trakhtenberg EF. The extent of extra-axonal tissue damage determines the levels of CSPG upregulation and the success of experimental axon regeneration in the CNS. *Sci Rep*. 2018;8 (1):9839.
47 Frade J, Nakagawa S, Cortes P, et al. Controlled ploidy reduction of pluripotent 4n cells generates 2n cells during mouse embryo development. *Sci Adv*. 2019;5(10):eaax4199.
48 Muller B, Wagner F, Lorenz B, Stieger K. Organotypic cultures of adult mouse retina: morphologic changes and gene expression. *Invest Ophthalmol Vis Sci*. 2017;58(4):1930–1940.
49 Madeira MH, Boia R, Elvas F, et al. Selective A2A receptor antagonist prevents microglia-mediated neuroinflammation and protects retinal ganglion cells from high intraocular pressure-induced transient ischemic injury. *Transl Res*. 2016;169:112–128.
50 Horn R. How ion channels sense membrane potential. *Proc Natl Acad Sci U S A*. 2005;102(14):4929–4930.
51 Vasylyev DV, Waxman SG. Membrane properties and electrogenesis in the distal axons of small dorsal root ganglion neurons in vitro. *J Neurophysiol*. 2012;108(3):729–740.
52 Yang CY, Tsai D, Guo T, et al. Differential electrical responses in retinal ganglion cell subtypes: effects of synaptic blockade and stimulating electrode location. *J Neural Eng*. 2018;15:(4) 046020.
53 Pannicke T, Bringmann A, Reichenbach A. Electrophysiological characterization of retinal Muller glial cells from mouse during postnatal development: comparison with rabbit cells. *Glia*. 2002;38 (3):268–272.
54 Felmy F, Pannicke T, Richt JA, Reichenbach A, Guenther E. Electrophysiological properties of rat retinal Muller (glial) cells in postnatally developing and in pathologically altered retinae. *Glia*. 2001;34(3):190–199.
55 Yin L, Geng Y, Osakada F, et al. Imaging light responses of retinal ganglion cells in the living mouse eye. *J Neurophysiol*. 2013;109 (9):2415–2421.
56 Zhong X, Gutierrez C, Xue T, et al. Generation of three-dimensional retinal tissue with functional photoreceptors from human iPSCs. *Nat Commun*. 2014;5:4047.
57 Silk AD, Gast CE, Davies PS, et al. Fusion between hematopoietic and epithelial cells in adult human intestine. *PLoS One*. 2013;8(1): e55572.

58 Theise ND, Nimmakayalu M, Gardner R, et al. Liver from bone marrow in humans. *Hepatology*. 2000;32(1):11–16.
59 Weimann JM, Charlton CA, Brazelton TR, Hackman RC, Blau HM. Contribution of transplanted bone marrow cells to Purkinje neurons in human adult brains. *Proc Natl Acad Sci U S A*.. 2003;100(4):2088–2093.
60 Goldenberg-Cohen N, Avraham-Lubin BC, Sadikov T, Askenasy N. Effect of coadministration of neuronal growth factors on neuroglial differentiation of bone marrow-derived stem cells in the ischemic retina. *Invest Ophthalmol Vis Sci*. 2014;55(1):502–512.
61 Tomita M, Mori T, Maruyama K, et al. A comparison of neural differentiation and retinal transplantation with bone marrow-derived cells and retinal progenitor cells. *Stem Cells*. 2006;24(10):2270–2278.
62 Xia J, Luo M, Ni N, Chen J, Hu Y, Deng Y, et al. Bone marrow mesenchymal stem cells stimulate proliferation and neuronal differentiation of retinal progenitor cells. *PLoS One*. 2013;8(9):e76157.
63 Abbuehl JP, Tatarova Z, Held W, Huelsken J. Long-term engraftment of primary bone marrow stromal cells repairs niche damage and improves hematopoietic stem cell transplantation. *Cell Stem Cell*. 2017;21(2):241–255. e6.
64 Arjmand B, Goodarzi P, Aghayan HR, et al. Co-transplantation of human fetal mesenchymal and hematopoietic stem cells in Type 1 diabetic mice model. *Front Endocrinol (Lausanne)*. 2019;10:761.
65 Kiani AA, Abdi J, Halabian R, et al. Over expression of HIF-1alpha in human mesenchymal stem cells increases their supportive functions for hematopoietic stem cells in an experimental co-culture model. *Hematology*. 2014;19(2):85–98.
66 Park HW, Kim YC, Yu B, et al. Alternative Wnt signaling activates YAP/TAZ. *Cell*. 2015;162(4):780–794.
67 Rueda EM, Hall BM, Hill MC, et al. The hippo pathway blocks mammalian retinal Muller glial cell reprogramming. *Cell Rep*. 2019;27(6):1637–1649. e6.
68 Lockery SR, Goodman MB, Faumont S. First report of action potentials in a C. elegans neuron is premature. *Nat Neurosci*. 2009;12(4):365–366. author reply 6.
69 Zhang X, Zhang M, Laties AM, Mitchell CH. Stimulation of P2X7 receptors elevates Ca^{2+} and kills retinal ganglion cells. *Invest Ophthalmol Vis Sci*. 2005;46(6):2183–2191.
70 De Melo Reis RA, Schitine CS, Kofalvi A, et al. Functional identification of cell phenotypes differentiating from mice retinal neurospheres using single cell calcium imaging. *Cell Mol Neurobiol*. 2011;31(6):835–846.
71 Freitas HR, Isaac AR, Silva TM, et al. Cannabinoids induce cell death and promote P2X7 receptor signaling in retinal glial progenitors in culture. *Mol Neurobiol*. 2019;56(9):6472–6486.
72 Zhang PP, Zhang G, Zhou W, Weng SJ, Yang XL, Zhong YM. Signaling mechanism for modulation by ATP of glycine receptors on rat retinal ganglion cells. *Sci Rep*. 2016;6:28938.
73 Yale AR, Nourse JL, Lee KR, et al. Cell surface N-glycans influence electrophysiological properties and fate potential of neural stem cells. *Stem Cell Rep*. 2018;11(4):869–882.
74 Eiraku M, Takata N, Ishibashi H, et al. Self-organizing optic-cup morphogenesis in three-dimensional culture. *Nature*. 2011;472(7341):51–56.
75 Sridhar A, Hoshino A, Finkbeiner CR, et al. Single-cell transcriptomic comparison of human fetal retina, hPSC-derived retinal organoids, and long-term retinal cultures. *Cell Rep*. 2020;30(5):1644–1659. e4.
76 Cowan CS, Renner M, De Gennaro M, et al. Cell types of the human retina and its organoids at single-cell resolution. *Cell*. 2020;182(6):1623–1640. e34.
77 Brancati G, Treutlein B, Camp JG. Resolving neurodevelopmental and vision disorders using organoid single-cell multi-omics. *Neuron*. 2020;107(6):1000–1013.
78 Livet J, Weissman TA, Kang H, et al. Transgenic strategies for combinatorial expression of fluorescent proteins in the nervous system. *Nature*. 2007;450(7166):56–62.
79 Weissman TA, Pan YA. Brainbow: new resources and emerging biological applications for multicolor genetic labeling and analysis. *Genetics*. 2015;199(2):293–306.
80 Hambright D, Park KY, Brooks M, McKay R, Swaroop A, Nasonkin IO. Long-term survival and differentiation of retinal neurons derived from human embryonic stem cell lines in un-immunosuppressed mouse retina. *Mol Vis*. 2012;18:920–936.
81 Lamba DA, Gust J, Reh TA. Transplantation of human embryonic stem cell-derived photoreceptors restores some visual function in Crx-deficient mice. *Cell Stem Cell*. 2009;4(1):73–79.
82 Lin B, McLelland BT, Mathur A, Aramant RB, Seiler MJ. Sheets of human retinal progenitor transplants improve vision in rats with severe retinal degeneration. *Exp Eye Res*. 2018;174:13–28.
83 Mitrousis N, Hacibekiroglu S, Ho MT, et al. Hydrogel-mediated co-transplantation of retinal pigmented epithelium and photoreceptors restores vision in an animal model of advanced retinal degeneration. *Biomaterials*. 2020;257: 120233.
84 Bielski CM, Zehir A, Penson AV, et al. Genome doubling shapes the evolution and prognosis of advanced cancers. *Nat Genet*. 2018;50(8):1189–1195.
85 Delespaul L, Merle C, Lesluyes T, et al. Fusion-mediated chromosomal instability promotes aneuploidy patterns that resemble human tumors. *Oncogene*. 2019;38(33):6083–6094.
86 Duncan AW, Hickey RD, Paulk NK, et al. Ploidy reductions in murine fusion-derived hepatocytes. *PLoS Genet*. 2009;5:(2)e1000385.